# REPORT DOCUMENTATION PAGE

Form Approved OMB No. 0704-0188



| 1. AGENCY USE ONLY (Leave blank) | 2. REPORT DATE | 3. REPORT TYPE AND DATES COVERED |
|---|---|---|
| | 1997 | Final Report |

4. TITLE AND SUBTITLE

Terabyte Holographic Memory

5. FUNDING NUMBERS

F6170896W0308

6. AUTHOR(S)

Dr. Mikhail Petrov

7. PERFORMING ORGANIZATION NAME(S) AND ADDRESS(ES)

A.F. Ioffe Physical Technical Institute
Polyteknicheskaya, 26
St. Petersberg 194021
Russia

8. PERFORMING ORGANIZATION REPORT NUMBER

N/A

9. SPONSORING/MONITORING AGENCY NAME(S) AND ADDRESS(ES)

EOARD
PSC 802 BOX 14
FPO 09499-0200

10. SPONSORING/MONITORING AGENCY REPORT NUMBER

SPC 96-4083



11. SUPPLEMENTARY NOTES

12a. DISTRIBUTION/AVAILABILITY STATEMENT

Approved for public release; distribution is unlimited.



12b. DISTRIBUTION CODE

A

13. ABSTRACT (Maximum 200 words)

This report results from a contract tasking A.F. Ioffe Physical Technical Institute as follows: Topic description: The following problems have been studied:

1. Spectral selectivity and multiplexing in volume holograms recorded in photorefractive materials.
2. Electric field multiplexing when recording and retrieving information in volume holograms having an external electric field.
3. Analysis of cross-talk and optical scattering in photorefractive materials that limit the maximum information capacity in volume holograms using spectral and electric field multiplexing.

The main results of the investigation are:

1. The main limiting factors on the magnitude of the electric field multiplexing are: inhomogeneity of the electric field in the crystal; the presence of the ordinary polarization in the illuminating light during readout of holograms; the magnitude of the breakdown in the electric field.
2. It was shown that the non-ideal coherence of the laser light used for hologram readout can play a very important role in cross-talk in spectral multiplexing. The experiment showed high spelectivity of volume holograms in $LiNbO_3$ have been carried out and validated the theoretical analysis.
3. A draft of a holographic memory system with a 1-Terabyte capacity has been proposed.

14. SUBJECT TERMS

Electronic Devices

15. NUMBER OF PAGES

78

16. PRICE CODE

N/A

| 17. SECURITY CLASSIFICATION OF REPORT | 18. SECURITY CLASSIFICATION OF THIS PAGE | 19. SECURITY CLASSIFICATION OF ABSTRACT | 20. LIMITATION OF ABSTRACT |
|---|---|---|---|
| UNCLASSIFIED | UNCLASSIFIED | UNCLASSIFIED | UL |

Ioffe Physico-Technical Institute

Russian Academy of Sciences

St. Petersburg

# Terabyte Holographic Memory

Contract F61708-96-W0308

## Final Report

Contractor

Prof. Dr. Mikhail Petrov

Fax:007-812-5156747

Tel:007-812-2479336

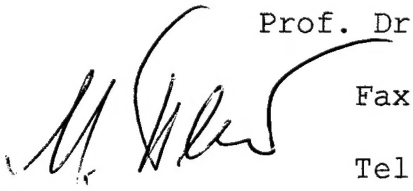

St.Petersburg

1997

Table of Contents


*Introduction* 3

*Chapter 1. Principles of Multiplexing in Volume Holograms* 6

*Chapter 2. Diffraction from Volume Holograms* 10

1. *readout Spectral selectivity and multiplexing* 12

2. *Experimental investigations of spectral selectivity of volume holograms* 13

3. *Cross-talk at spectral multiplexing* 24

   a) *Cross-talk caused by the complicated structure of the recorded image in case of ideally coherent readout light.* 24

   b) *Cross-talk caused by nonmonochromatic light* 30

*Chapter 3. Electric Field Selectivity and Multiplexing* 45

*Chapter 4. Dynamic Range and Light Scattering from Volume Holograms* 63

*Chapter 5. Holographic Memory System Configuration* 67

*Conclusions* 72

*References* 75

## *Introduction*

In accordance with contract F61708-96-W0308 the following problems have been studied:

1. Spectral selectivity and multiplexing in volume holograms recorded in photorefractive materials.
2. Electric field multiplexing when recording and retrieving information in volume holograms having an external electric field.
3. Analysis of cross-talk and optical scattering in photorefractive materials that limit the maximum information capacity in volume holograms using spectral and electric field multiplexing.

During the first six months the major part of the investigations concerning the electric field multiplexing was carried out and a detailed description was presented in the Interim Report [1]. So in the final report we mostly present the investigations of spectral selectivity and multiplexing in volume holograms using photorefractive materials. We analyze the cross-talk and optical scattering in photorefractive materials that limit the maximum information capacity in volume holograms using spectral multiplexing. Then we present the final results concerning electric field multiplexing. In addition to this, we propose a draft of a holographic memory

system using spectral and electric field multiplexing and having potentially 1-Terabyte capacity of the memory.

The main results of the investigation according the contract are:

1. The theoretical analysis of electric field multiplexing and selectivity was made for the photorefractive $LiNbO_3$ crystal. The optimal configuration for the electric field multiplexing was found.

   The experimental investigations of the electric field multiplexing have shown that the main factors limiting the magnitude of the electric field multiplexing are as follows:

   - inhomogeneity of the electric field in the crystal;
   - the presence of the ordinary polarization in the illuminating light during readout of holograms;
   - the magnitude of breakdown electric field.

   The conclusion was made that the value of electric field multiplexing

   $$M_{ef} = 10 \div 20$$

   is realistic.

2. Various sources of cross-talk at spectral multiplexing were analyzed. It was shown that a non-ideal coherence of the laser light used for hologram readout can play a very important role in cross-talk in spectral multiplexing. The necessary criteria for the spectral bandwidth of the

readout light were found.

The experiments demonstrating a high spectral selectivity of volume holograms in $LiNbO_3$ have been carried out and have showed the correctness of the theoretical analysis.

3) The important role of light scattering in reducing the dynamic range, spatial bandwidth of a hologram, and information capacity of the holographic memory system have been discussed. A draft of a holographic memory system with a 1-*Terabyte* capacity has been proposed.

So all the required investigations in accordance with the conditions of the contract have been carried out and new scientific results have been obtained.

The recommendations for further investigations in the area of holographic memory have been drawn.

## *Chapter 1. Principles of multiplexing in volume holograms*

During the last few years a remarkable progress in the development of holographic memories was made. For instance, the demonstrator with the information capacity of ~ 1 *Gbytes* was built [2].

However, a radical increase in the information capacity is desirable to make a system competitive with other archive storage systems.

To this end, serious problems are to be solved. Among them are the problems of an appropriate holographic material and optimal system of hologram multiplexing. The term «hologram multiplexing» may have different meanings. The term «spatial multiplexing of holograms» means recording of different holograms in the spatially separated areas (or pieces) of photosensitive materials, whereas other forms of multiplexing (angular, spectral, phase code, electric field) mean recording of different holograms in the same volume of the material, but under different conditions of recording.

Up to now the most thoroughly studied techniques of multiplexing have been angular and phase code ones [3-20]. In the case of angular multiplexing holograms are recorded at corresponding angles of the reference beam [2-15]. In the case of phase code multiplexing the recording occurs at different spatial phase modulations of the cross-section of the reference beam [5,16-20]. These two techniques can be

relatively easily realized because well-developed acousto-optical deflectors and liquid crystal spatial light modulators are commercially available. However, the angular and phase code multiplexing are not independent because the same degree of freedom (angles of the reference laser beam propagation) is exploited here. That is why a simultaneous use of both techniques does not increase the information capacity of the holographic system. Nevertheless, they can provide some interesting specific advantages in the construction of the system.

The less studied technique of multiplexing is the spectral one [21-25]. This is because the spectral multiplexing requires tunable highly coherent lasers with fast switching which are not available at present. However, a considerable progress in the development of tunable lasers has been made in recent years, especially in the areas of semiconductor lasers, OPO-lasers, and some other solid state lasers [26-28]. So it is quite reasonable to expect that fast switching tunable lasers will appear on the market in future. That is why more detailed investigations of the potential of wavelength (spectral) multiplexing are of particular interest now. In [21,22,29], very important advantages of spectral multiplexing over the angular one were noted. The most significant advantage is a lower cross-talk between pages of information. According to [29], the cross-talk between pages of information recorded at different wavelengths at spectral

multiplexing is proportional to the ratio $(K_{g\perp max}/K_g)^2$, where $K_{g\perp max}$ is the hologram wave vector component which presents the maximum spatial frequency of the recorded image and $K_g$ is the wave vector of the grating which corresponds to the «carrier spatial frequency» of the holographic grating. So the higher information capacity of the page, the higher the ratio $K_{g\perp max}/K_g$. A reasonable ratio $K_{g\perp max}/K_g$ is of the order of $10^{-1}\div10^{-2}$, and hence the noise-to-signal ratio is of the order of $10^{-2}\div10^{-4}$. However, for angular multiplexing the cross-talk is proportional to $K_{g\perp max}/K_g$. That is why the cross-talk for angular multiplexing can potentially limit the amount of information which can be recorded in one page, whereas spectral multiplexing allows recording of a much greater volume of information in one page. This can be very useful for elaboration of more effective architectures of the holographic memory. However, as it will be shown below, spectral multiplexing is very «sensitive» to spectral characteristics of the reference laser beam to be used for readout. If the spectrum of the reference beam is not narrow enough, enormous cross-talk can result and this can make the use of spectral multiplexing almost impossible. This problem has been studied in detail in this project for the first time and is presented in this report.

In this project we study one more type of multiplexing which allows one to use one more degree of freedom. This is a

change of the refractive index of a holographic material by applying an external electric field. Since the volume holographic memory described here is based on photorefractive crystals which are electrooptic materials, application of an external electric field to these crystals results in a change in the refractive index and, hence, a change in the Bragg conditions (1). One of the most important advantages of this multiplexing technique is its very simple realization when electrooptic photosensitive holographic media are used because one needs merely to apply different electric fields to record and reconstruct different holograms.

Formally, the refractive index $n_a$ and wavelength $\lambda$ are absolutely independent variables, but they are connected by the Bragg conditions. So degenerate states are possible when variation in $n_a$ can be compensated by such variation in $\lambda$ that the Bragg condition (1) is satisfied. So the necessary compromise in using the spectral and electric field multiplexing must be found for each particular architecture of holographic memory. In this report a detailed investigation of electric field multiplexing is described.

## *Chapter 2. Diffraction from Volume Holograms*

A high-density holographic storage relies on the volume character of recording of information in thick photosensitive materials. Diffraction from volume holograms obeys the Bragg condition (Fig.1)

$$\vec{K}_g = \pm(\vec{\rho} - \vec{\sigma}_i) \tag{1}$$

or

$$\left|\vec{K}_g\right| = 2 \cdot \frac{2\pi}{\lambda} n_a \sin\theta_0 = \frac{2\pi}{\Lambda} \tag{2}$$

Here, $\left|\vec{K}_g\right|$ is the wave vector of the holographic grating (the simplest hologram), $\lambda$ is the light wavelength in air, $\theta_0$ is the Bragg angle in the material, $n_a$ is the average refractive index, $\Lambda$ is the holographic grating period, and $\vec{\rho}$ and $\vec{\sigma}_i$ are the wave vectors of the reference and object beams, respectively. Expression (2) establishes the relationship between $\theta_0$, $\lambda$, and $n_a$ for the hologram with infinite sizes. When the hologram thickness $T$ is finite, the condition (2) can be violated to some extent, which means that the angle of incidence of the reference beam $\theta$, wavelength $\lambda$, or the refractive index $n_a$ at readout can differ slightly from those at recording. The magnitude of possible variations in $\theta$, $\lambda$, or $n_a$ is the measure of corresponding selectivity (spectral, angular, refractive index). The analysis of the diffraction efficiency of volume holograms as a function of detuning of $\theta$

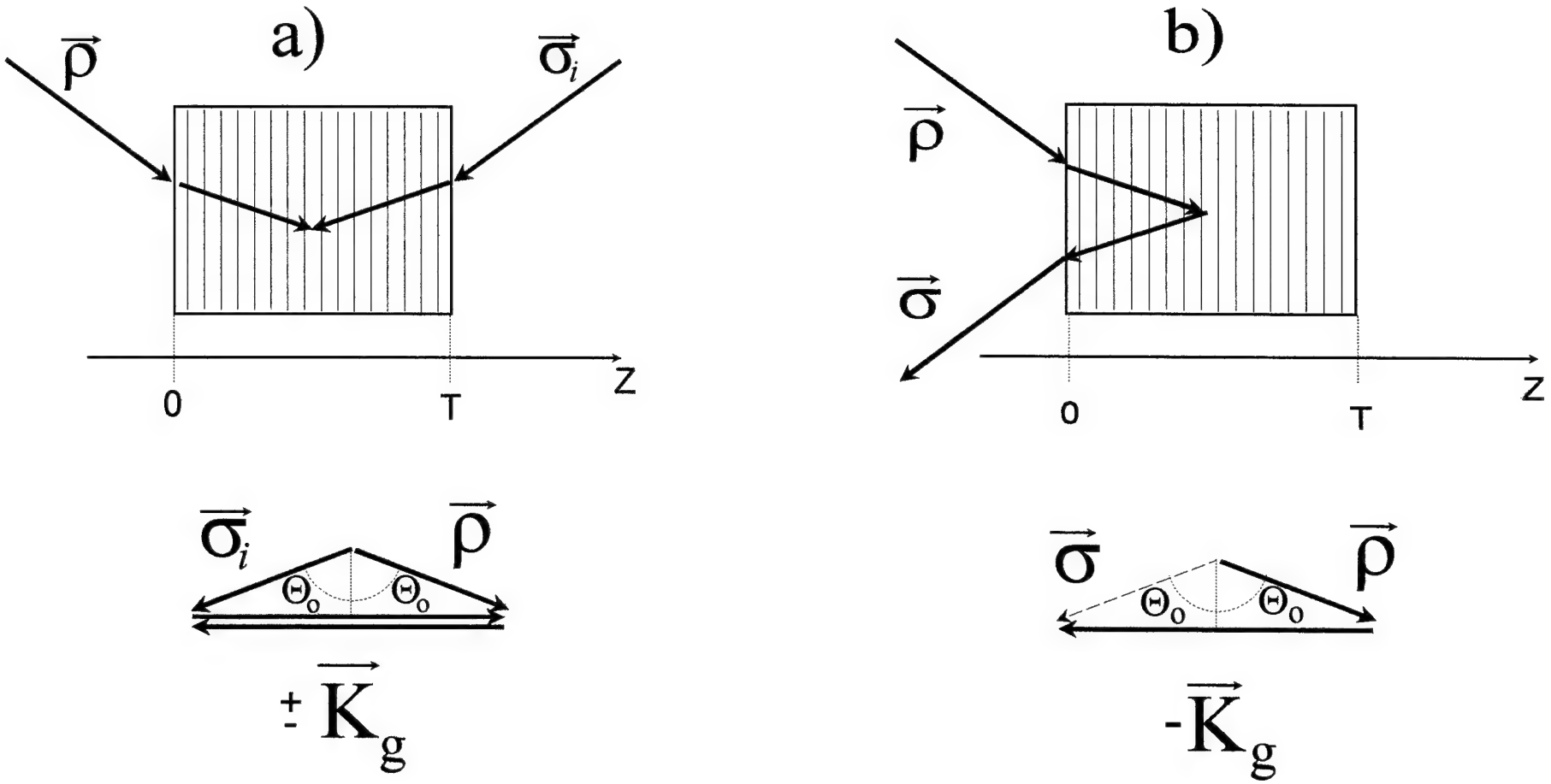


Fig.1 a) The geometry for recording of reflection volume holograms; b) The geometry for readout of reflection volume holograms.

and λ was made by Kogelnik [30]. There are different results for transmission and reflection volume holograms. Since the spectral selectivity for reflection holograms is higher, we shall discuss just this type of holograms.

*Spectral selectivity and multiplexing*

Let us consider the refractive index sinusoidal grating

$$n(z) = n_a + n_1 \cos(K_g z) \tag{3}$$

in a thick material with thickness $T$ and transverse dimensions much larger than $T$. Then expression for the diffraction efficiency of the reflection hologram is [30]

$$\eta = \left| \frac{1}{(i\xi_r/\nu_r) + \left[1 - (\xi_r/\nu_r)^2\right]^{1/2} cth\left(\nu_r^2 - \xi_r^2\right)^{1/2}} \right|^2 \tag{4}$$

Here

$$\xi_r = -\frac{\Delta\lambda}{\lambda_r}\beta T \sin\theta_0 \tag{5}$$

$$\nu_r = \frac{\pi \cdot n_1 T}{\lambda_r \sin\theta_0} \tag{6}$$

$$\beta = K n_a = \frac{2\pi}{\lambda_r} n_a \tag{7}$$

and

$$\Delta\lambda = \lambda_w - \lambda_r \tag{8}$$

is the wavelength detuning, and $\lambda_w$ and $\lambda_r$ are the wavelengths at recording and readout of holograms.

Since we consider the system where a large number $M$ of holograms is recorded in the same volume of a material, it should be borne in mind that the diffraction efficiency varies as $\sim 1/M^2$ and, hence, $n_1 << 1$ and $\nu_r << 1$. Then the diffraction efficiency goes to its first zero at $\xi_r = \pi$. Let us denote the difference $\lambda_w - \lambda_{r0}$ by $\Delta\lambda_0$, where $\lambda_{r0}$ is the wavelengths at which the diffraction efficiency $\eta$ has a zero value. It follows from (5) that

$$\frac{\Delta\lambda_0}{\lambda_r} = \frac{\lambda_r}{2Tn_a \sin\theta}, \text{ or } \frac{\Delta\lambda_0}{\lambda_r} = \frac{\Lambda}{T} \qquad (9)$$

For the numerical estimation of selectivity we use $T = 1$ cm, $\lambda_r = 633$ nm, $\theta = 90^0$, and $n_a = 2.23$. Then $\frac{\Delta\lambda_0}{\lambda_r} = 1.42 \cdot 10^{-5}$. So the theoretical magnitude of spectral multiplexing is $M_s = \frac{\lambda_{max} - \lambda_{min}}{\Delta\lambda_0} = 1.4 \cdot 10^3$ if $\frac{\lambda_{max} - \lambda_{min}}{\lambda_r} \approx 10^{-2}$. Here, $\lambda_{max} - \lambda_{min}$ is the total range of tuning. Here we used the wavelength scale instead of the frequency scale to estimate the tuning range because of a narrow band of tuning.

*Experimental investigations of spectral selectivity of volume holograms*

To demonstrate spectral selectivity and estimate the magnitude of the experimental spectral multiplexing, the following experiments were carried out.

A single crystal of $LiNbO_3$ $1.82 \times 4.09 \times 5.06\ mm^3$ in size was used (Fig.2). The specific holographic orientation for the reflection geometry was selected. The *"C"* axis of the crystal was oriented along the longest edge of the sample. The holograms were recorded in a nearly conterpropagating geometry when the incident angles for different holograms were $\alpha = 90^0 - \theta_0$, the particular values of $\alpha$ being $\alpha_1 \approx 2^0 30'$ ; $\alpha_2 \approx 2^0 15'$ ; $\alpha_3 \approx 2^0 7'$ (Fig.2).

Simple gratings were recorded using a He-Ne laser. Since the elementary holograms (simple sinusoidal gratings) were recorded, the reconstruction could be carried out at a fixed incidence angle, but with different wavelengths of the readout light for the holograms with different grating spacings. The noncoherent source (a well-calibrated monochromator) was used for readout of holograms. The setup for readout is shown in Fig.3. The light source is a mercury lamp. The rotation of the monochromator grating 5 results in a change of the light wavelength at the output of the monochromator. Then the output light is modulated by a shutter (10) and illuminates the crystal where one or several holograms have been recorded. The diffracted light is detected by a photomultiplier (13). This setup was used for demonstrating the wavelength selectivity, however, it will allow us in the future to make measurements of cross-talk as a function of the coherence of the readout light and thus to check the theoretical conclusions which were made in this work.

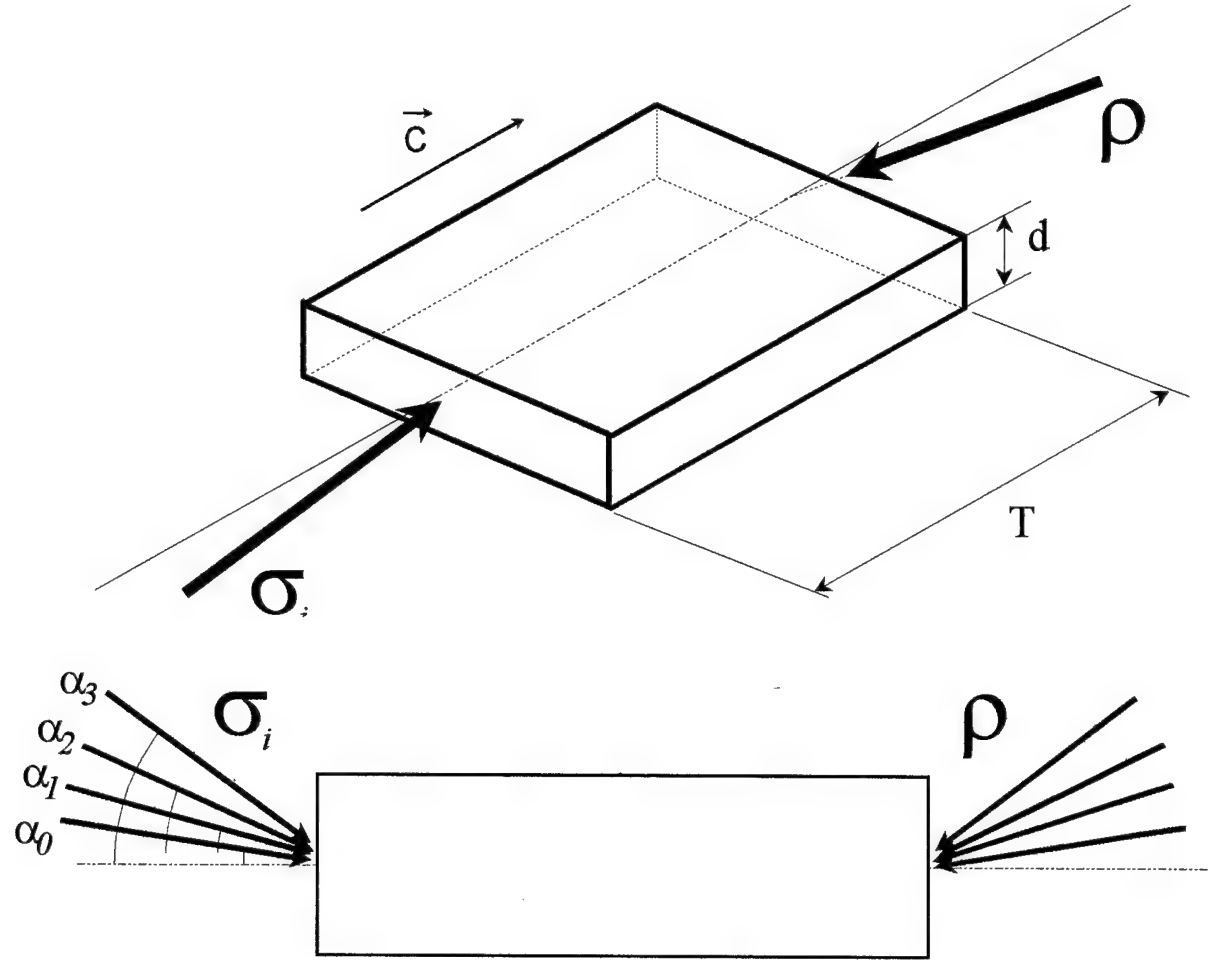


Fig.2 The orientation of the LiNbO crystal used in the experiments on investigation of wavelength selectivity.

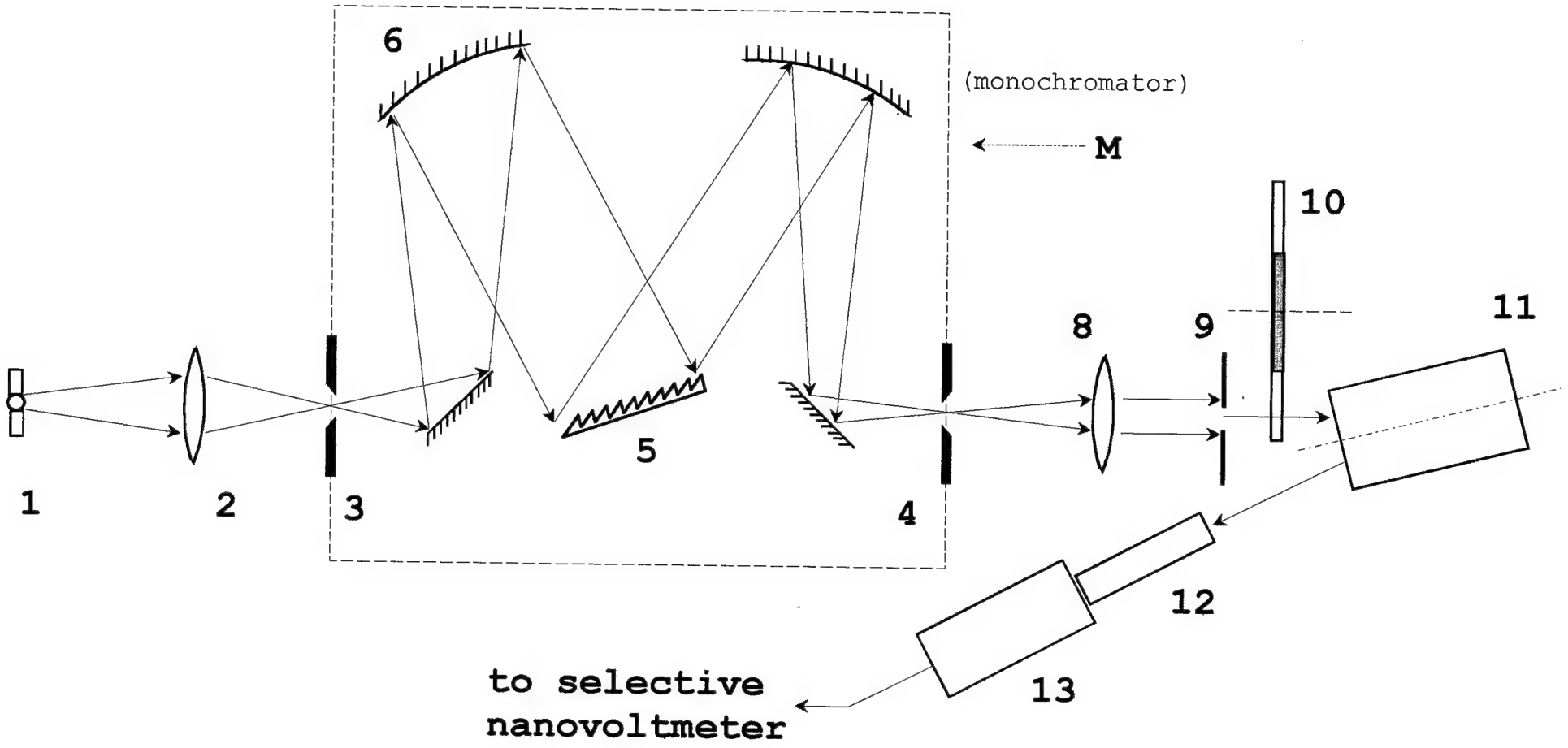


Fig.3 Experimental setup: 1- mercury lamp; 2-cylindrical lens; 3-input slit; 4-output slit; 5-grating; 6,7-spherical mirrors; 8-cylindrical lens; 9-diaphragm; 10-shutter; 11-sample; 12-microscope; 13-photomultiplier.

Fig.4 shows the spectrum of the output light when a He-Ne laser is used instead of a mercury lamp. So the transfer function of the monochromator was measured when the orientation of grating (5) was changed. Because of the preliminary calibration of the monochromator, we can present the intensity of the output light as a function of wavelength. From this figure it is seen that the resolution (the interval between central maximum and the nearest minimum) is approximately $0.15\,\mathring{\mathrm{A}}$.

Using the relationship (9) one can estimate the spectral selectivity of the recorded hologram in the $LiNbO_3$ crystal used and we can find

$$\Delta\lambda_0 = \frac{\lambda_r \Lambda}{T} \approx 0.2\,\mathring{\mathrm{A}} \qquad (10)$$

Here, $T = 5\ \mathrm{mm}$, $\lambda_r = 633\ \mathrm{nm}$. The experimental data for different situations are shown in Figs.5,6,7 and 8. The intensity of diffracted light as a function of $\Delta\lambda$ of the readout light for the cases when one or two gratings are recorded is shown in these figures.

It is seen from Fig.5 that the spectral interval between the central maximum and the first zero (minimum) is equal to approximately $0.5\,\mathring{\mathrm{A}}$. The output signal is a convolution

$$I_{out}(\lambda_r) = \int_{-\infty}^{\infty} I_h(\lambda') I_m(\lambda_r - \lambda')\, d\lambda' \qquad (11)$$

where $I_h(\lambda')$ is the spectral characteristic of the recorded hologram, and $I_m(\lambda_r - \lambda')$ is the transfer function of the monochromator (Fig.4). From the experimental data (Figs.5 and

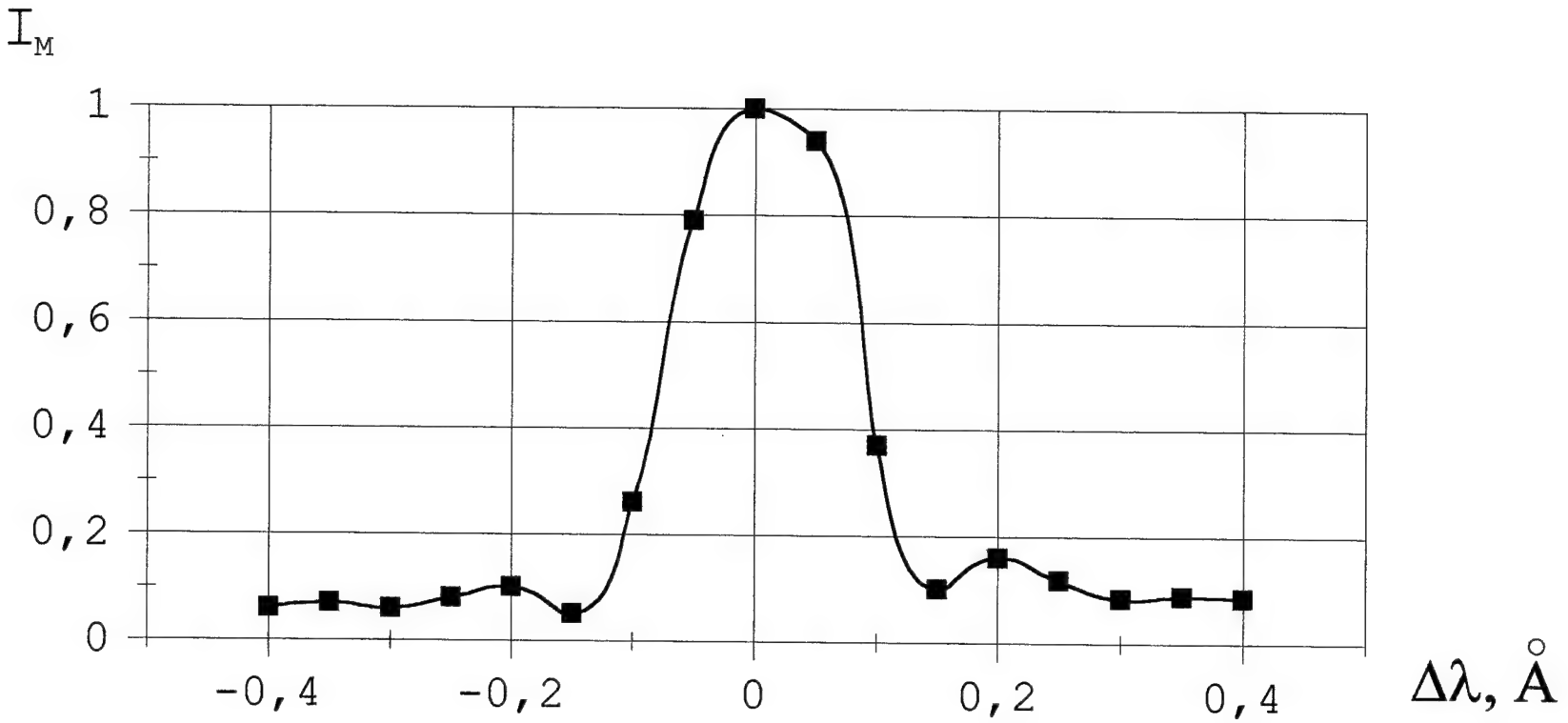


Fig.4 Transfer function of the monochromator.

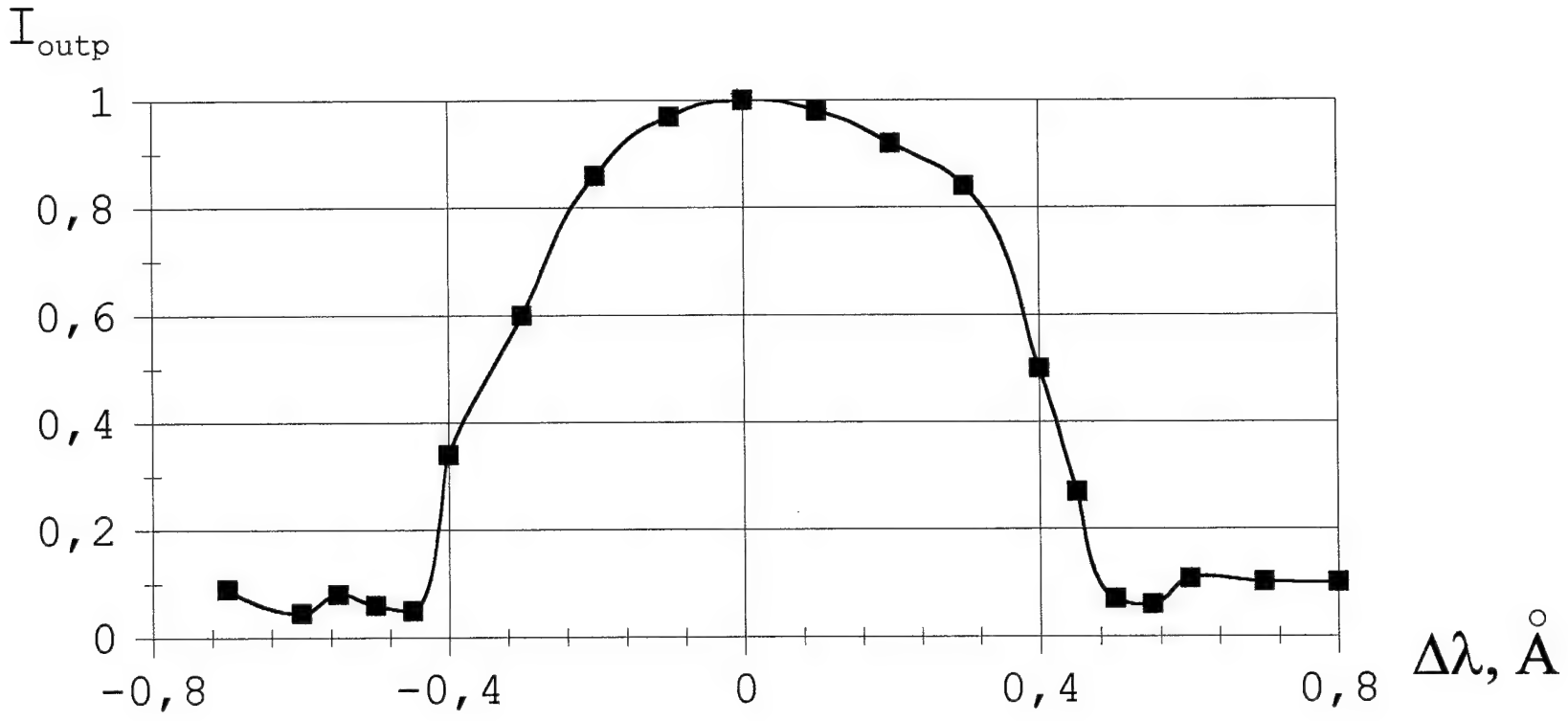


Fig.5 The output signal as a function of detuning Δλ.

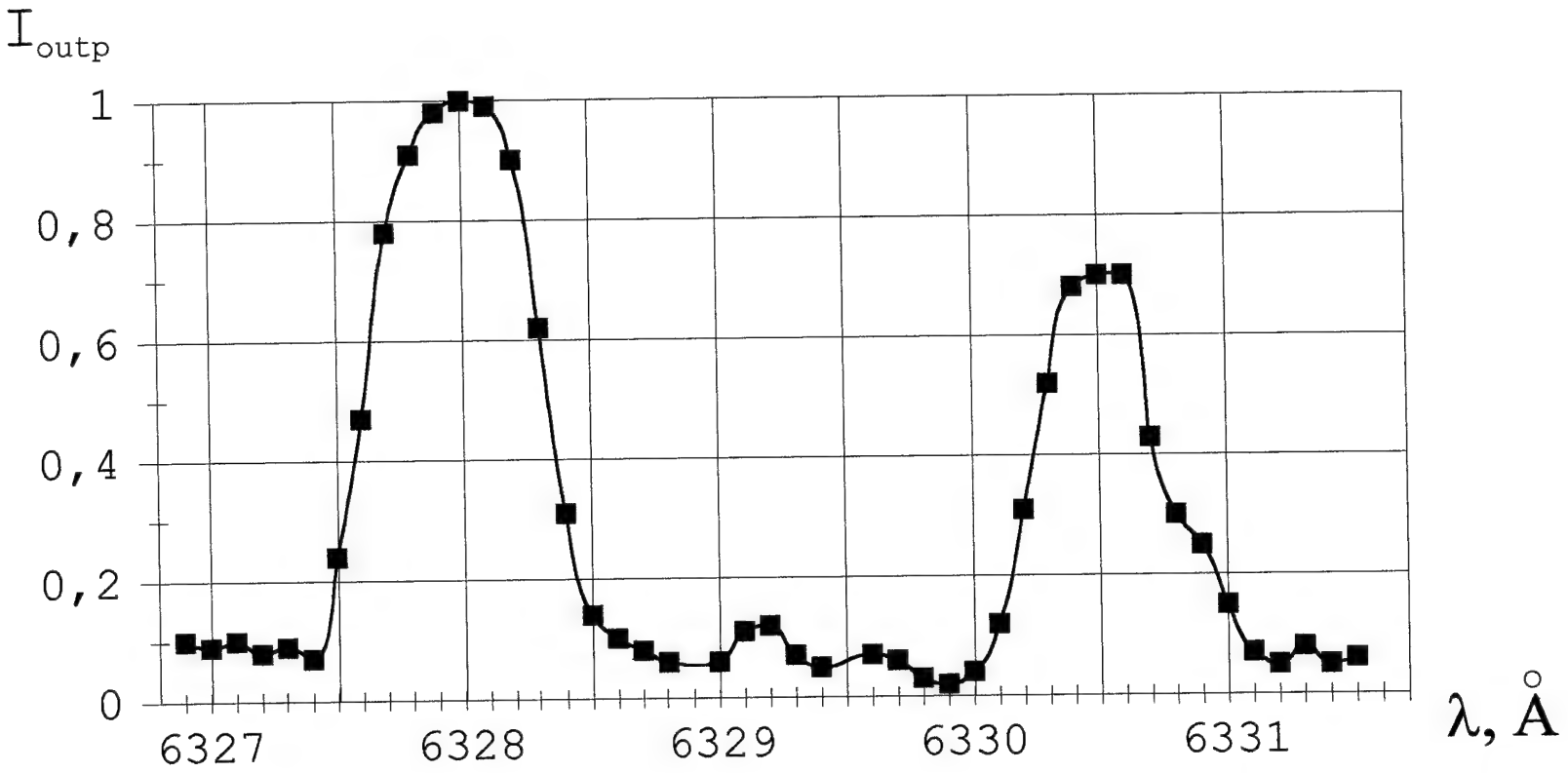


Fig.6 The output signal as a function of wavelength of readout light for the case when two holograms are recorded at different angles $\alpha_0$ and $\alpha_3$.

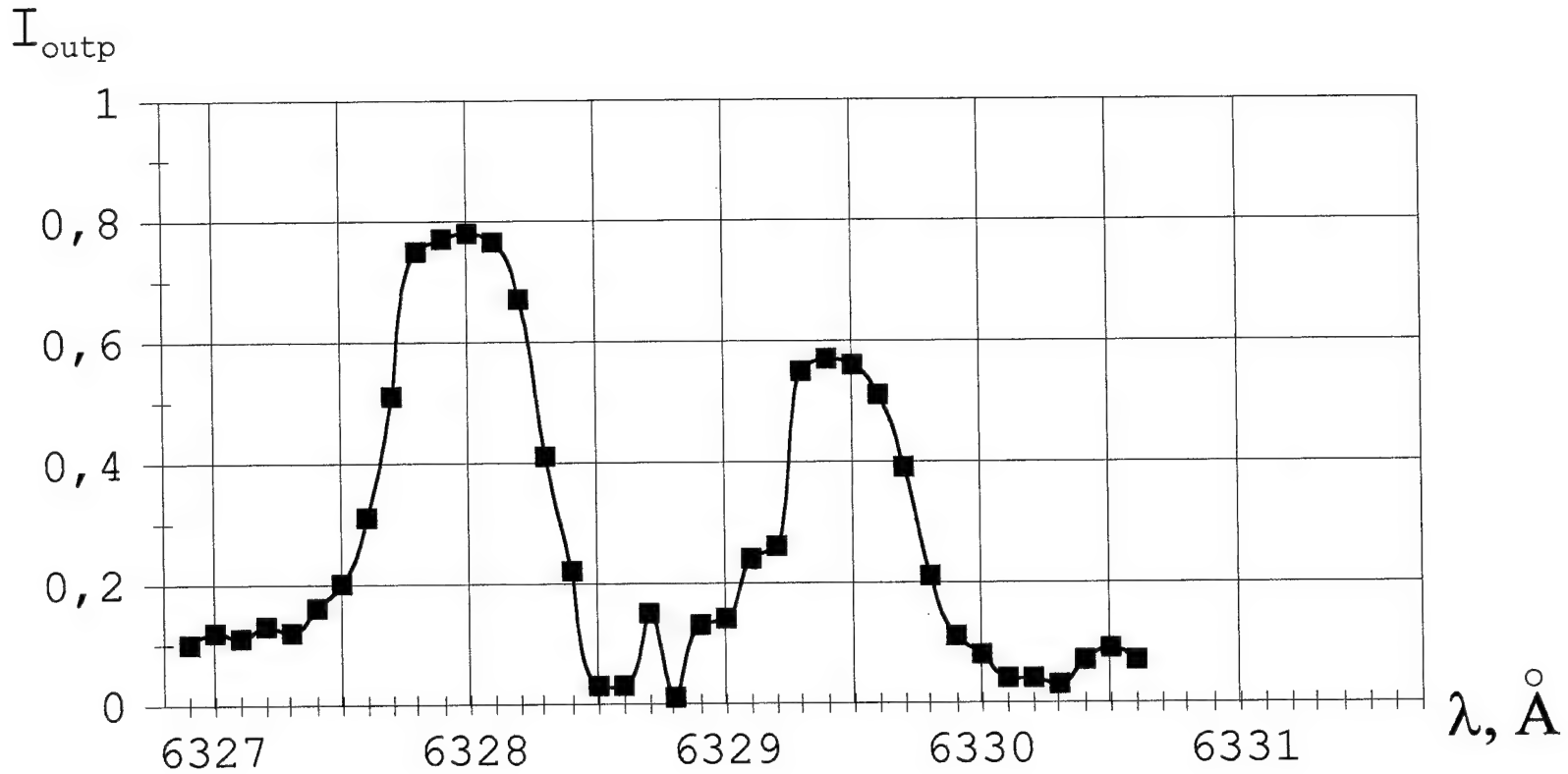


Fig.7 The output signal as a function of wavelength of readout light for the case when two holograms are recorded at different angles $\alpha_0$ and $\alpha_2$.

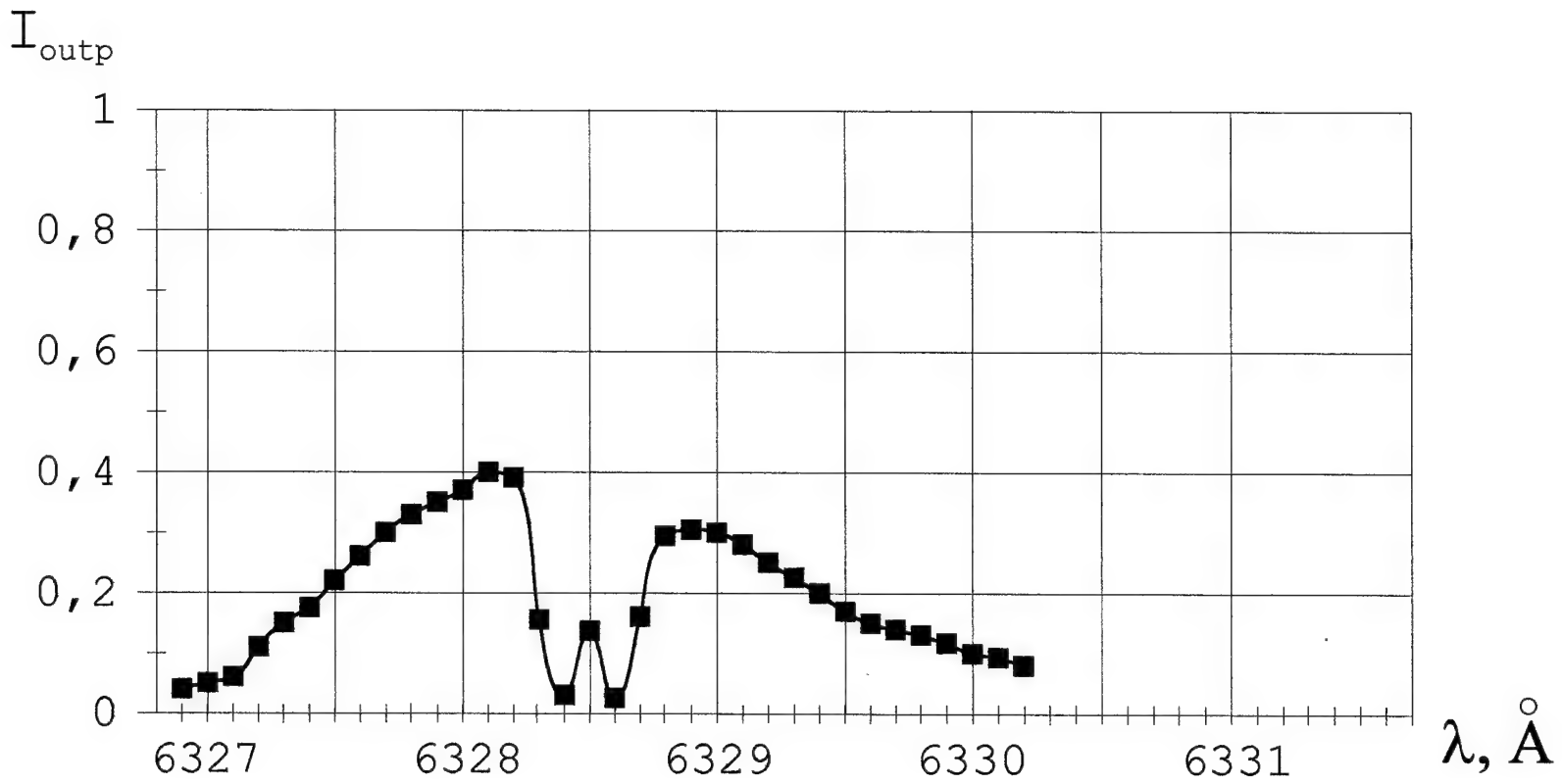


Fig.8 The output signal as a function of wavelength of readout light for the case when two holograms are recorded at different angles $\alpha_0$ and $\alpha_1$.

4), it is easy to estimate the experimental value of $\Delta\lambda_0$ for the hologram. It was found from such estimations that $\Delta\lambda_0$ = 0.3÷0.35. This value can be regarded as a qualitative agreement with the theoretical value of $0.2\,\mathring{A}$ (10). The observed difference between the theoretical and experimental values can be explained by at least two factors:

- the actual thickness of the hologram is smaller than the crystal thickness because of a nonideal overlap of the recording beams;
- the holograms amplitude varies along the *z* axis because of light absorption.

More detailed investigations are required to reach the theoretical limit in $\Delta\lambda_0$ for really thick holograms. However, for the preliminary experiment, the obtained result can be regarded as acceptable.

Figs.6-8 clearly show that two holograms are very well separated when the distance between the maxima is appr. $1\div1.5\,\mathring{A}$. This means that if we want to have the spectral multiplexing $M_s$ of the order of $10^3$ for the sample under study, we need the total tuning range of the wavelength of the order of 20÷25% from the wavelength of the He-Ne laser. This range potentially can be even more narrow if thicker holograms are used.

## *Cross-talk at spectral multiplexing*

It follows from (4-9) that if one simple hologram (grating) is recorded at $\lambda_w$ and the other one at $\lambda_{r0}$, then during reconstruction at $\lambda_w$ only the first hologram will be read out and at illumination by $\lambda_{r0}$ only the second one will be reconstructed. So for a simple grating and if the reconstructing light with an infinite narrow spectrum is used (at $\lambda_w$ or $\lambda_{r0}$), no cross-talk between these two holograms results. However, it is not true for complicated holograms or for the reconstructing beam with the finite spectrum.

*a) Cross-talk caused by the complicated structure of the recorded image in case of ideally coherent readout light.*

It is seen from (5) that the position of the zero value of diffraction efficiency depends on $K_g$ . So in case the complicated holograms which contain different $K_g$ are recorded at $\lambda_w$, the condition (9) cannot be satisfied for all gratings simultaneously because $\Delta\lambda_0$ is different for different gratings (Fig.9). That is why the cross-talk between two pages of information arises, i.e., if one page is recorded at $\lambda_w$ and the other is recorded at $\lambda_{r0}$, then during readout at $\lambda_w$ the pages which have been recorded at $\lambda_{r0}$ will be partially reconstructed and vice versa. The maximum variations in the length of $K_g$ are determined by $\Delta K_g$

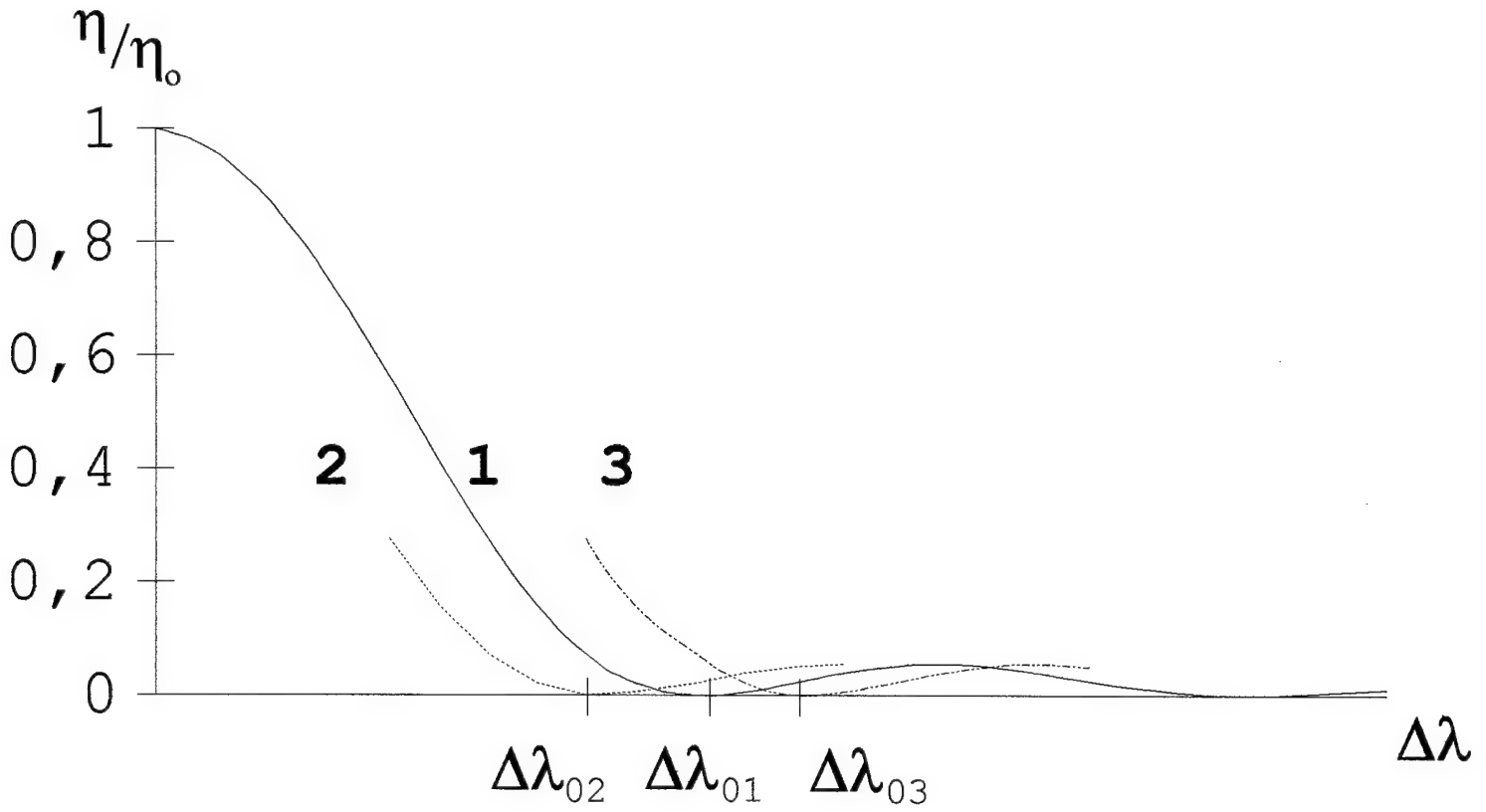


Fig.9 Diffraction efficiency (in AU) as a function of $\Delta\lambda$ for reflection volume holograms. 1 - $K_{g\perp}=0$ ; 2,3 - $K_{g\perp}\neq 0$.

$$\Delta K_g = \sqrt{K_{g0}^2 + K_{g\perp}^2} - K_{g0} = \frac{1}{2}\frac{K_{g\perp}^2}{K_g} \tag{12}$$

where $K_{g0}$ is the length of the grating wave vector for $K_{g\perp} = 0$. It is $K_{g\perp}$ that carries information about the recorded image. To find the cross-talk intensity (noise), we expand expression (4) in the Taylor series near point $\xi_r = \pi$.

Then

$$\Delta\eta(\xi_r = \pi) = \frac{1}{2}\frac{d^2\eta}{dK_g^2}\bigg|_{\xi_r=\pi} \cdot \left(\Delta K_g\right)^2 \tag{13}$$

$$\Delta\eta(\xi_r = \pi) = \frac{\nu_r^2}{4}\left(\frac{K_{g\perp}}{K_g}\right)^4 \tag{14}$$

The noise-to-signal ratio is

$$NSR = \frac{\Delta\eta(\xi_r = \pi)}{\eta(\xi_r = 0)} = \frac{1}{4}\left(\frac{K_{g\perp}}{K_g}\right)^4 \tag{15}$$

This is the result for two holograms. In the case of $M$ holograms separated by $\Delta\lambda_0$ from each other, the summation for high values of $M$ ($M' \approx \frac{K_{g\perp}}{K_g}$), i.e., when $M = 10^2 \div 10^3$, results in

$$NSR \sim \left(\frac{K_{g\perp}}{K_g}\right)^2 \tag{16}$$

For the case of $\frac{K_{g\perp}}{K_g} = 5 \cdot 10^{-2}$ that allows recording of appr. 300 pixels/mm when $\theta = 90^0$, the noise-to-signal ratio is of the order of $10^{-3}$. So this is quite a negligible effect. Rakuljic et al. [21] arrived at the same conclusion from some

qualitative considerations and their experimental results were consistent with this conclusion.

The same result can be obtained more rigorously. The detailed theoretical analysis was performed in [22,29] for the Fourier transform storage, i.e., when the Fourier transform of the initial image is stored. The expansion of the image into the plane wave is a key feature of this formalism. In [22], the coupled wave theory was used. The finite thickness over which the integration was carried out caused spatial frequency components other than $K_g$ to also yield nonzero contributions to the integral. The slowly varying amplitude approximation and the undepleted reference wave approximation lead to the expression for the amplitude of the reconstructed light wave:

$$a^{(l)}(\sigma_\perp) = \alpha_0 \cdot z A^{(l)}(\sigma_\perp) + \sum_{m \neq l}^{M} \alpha_1 \, sinc\left[\left(\beta_m - \beta_l\right) \cdot \left(1 + \frac{\sigma_\perp^2}{4\beta_m \beta_l}\right) z\right] A^{(m)}(\sigma_\perp) \quad (17)$$

where $\beta_m = 2\pi n_o / \lambda_{wm}$ is the wavevector magnitude at recording, and $\beta_l = 2\pi n_o / \lambda_{rl}$ is the wavevector magnitude at readout. $A^{(l)}(\sigma_\perp)$ and $a^{(l)}(\sigma_\perp)$ are the complex amplitudes of recording and readout signals, respectively. The first term on the right-hand side of Eq.(17) represents the reconstructed page $l$ without any cross-talk. The next term (the sum) accounts for the coherent cross-talk contributions from all the remaining recorded holograms. The weak dependence on $\sigma_\perp$ confirms the qualitative conclusions given above. This formalism can readily account for the role of the finite transverse dimensions of the

optical elements. In [29] the same result was obtained following the standard scalar diffraction theory and assuming that the Born and paraxial approximations are valid. The *NSR* is a convenient measure used to asses the cross-talk. To estimate the noise-to-signal ratio, they divided the total average noise power by the signal power. It was assumed that each pixel on the stored images is an independent random variable, taking the values of zero and one with equal probability. The *NSR* was calculated for the recording schedule that places the center of each image at the zero value of diffraction efficiency (in the wavelength space) of the adjacent hologram. The dependences on the total number of holograms and $\sigma_{\perp}$ were obtained by numerically evaluating. An asymptotic closed form expression for maximum *NSR* was derived for the reflection geometry:

$$NSR \approx \frac{\sigma_{\perp max}^2}{4\beta_l^2} \tag{18}$$

where $\sigma_{\perp max}$ can be expressed through the parameters of the Fourier optics: the Fourier transform lens depth of focus ($F$) and transverse dimensions $x_{\max}$ and $y_{\max}$ of the optical elements $\sigma_{\perp max} = \left( \sqrt{x_{max}^2 + y_{max}^2} \Big/ F \right) \cdot \beta_m$. In the limiting case, when the sizes of the image are equal to the sizes of the optical elements, for $\lambda_{w0}$=0.5μm, $x_{max} = y_{max} = 15\text{mm}$, and $F = 30\text{cm}$, $NSR^{-1}$ is more that 800 even in the worst case. This agrees with the conclusions made above ($NSR \approx 10^{-3}$). Note that the theoretical predictions for *NSR* given by (18) give the worst case value for the cross-talk and

are valid when the total number of holograms is of the order of $10^3$ or greater.

Several comments should be made here. First, there is no way to reduce the cross-talk noise to zero. Second, when $M$ is large, the worst cross-talk is seen to occur when the geometry deviates from the ideal case. For example, in the wavelength multiplexing the cross-talk is minimized in the counterpropagation geometry. The highest cross-talk noise occurs at the outermost signal pixels because the wave vectors corresponding to this pixel have maximal transverse components.

In [31], the cross-talk was examined when reference beams were sparsely selected and the wavelengths were separated by an amount greater than the wavelength selectivity of the recording medium. Let us introduce the following notations:

$$\beta_m = \frac{\pi(M_r - S\cdot m + 1)}{T}; \qquad 0 < S\cdot m \le M_r$$
$$S = \frac{\lambda_{wm} - \lambda_{wm+1}}{\Delta\lambda_0}; \qquad M_r = \frac{2n_a T}{\lambda_{wmin}} \tag{19}$$

It was shown that for the case when $S$ is an integer the sparse selection of the reference waves can lead to some improvement in the cross-talk in the wavelength-multiplexed systems at the cost of increasing the total wavelength tuning range.

In the wavelength multiplexing, the sparsely spaced reference beams remain counterpropagating, therefore there is no increase in the noise compared with the optimal geometry.

Sparse spacing decreases the total cross-talk by decreasing the noise contribution of the nearest neighbors since $S$ increases, and the number of wave vectors falling within one period of the sinc function in Eq.(17) decreases by a factor of $1/S$. Therefore, the improvement can be achieved if the laser source can be tuned over the increased wavelength range. In contrast of this, in angular multiplexing sparse selection of the reference beams involves increased deviation from the ideal geometry. The noise increase due to the geometrical dependence of the cross-talk cancels any advantage gained by increasing the angle separation of the holograms. However, in a system with inaccurate reference beam angular positioning sparse selection can offer some improvement in cross-talk performance.

All the results considered above have been obtained for readout by ideally coherent reference waves. However, the real tunable lasers (solid-state, OPO lasers, dye lasers, semiconductor lasers) have a limited coherence. Intuitively, it is clear that the use of nonmonochromatic readout light could increase cross-talk. In this work we study the cross-talk when the readout light is not monochromatic.

*b. Cross-talk caused by nonmonochromatic readout light*

We examine a slab medium whose thickness is in the $z$ dimension and whose infinite lateral extents are in the $x$ and $y$ dimensions as shown in Fig.10. Consider the volume hologram

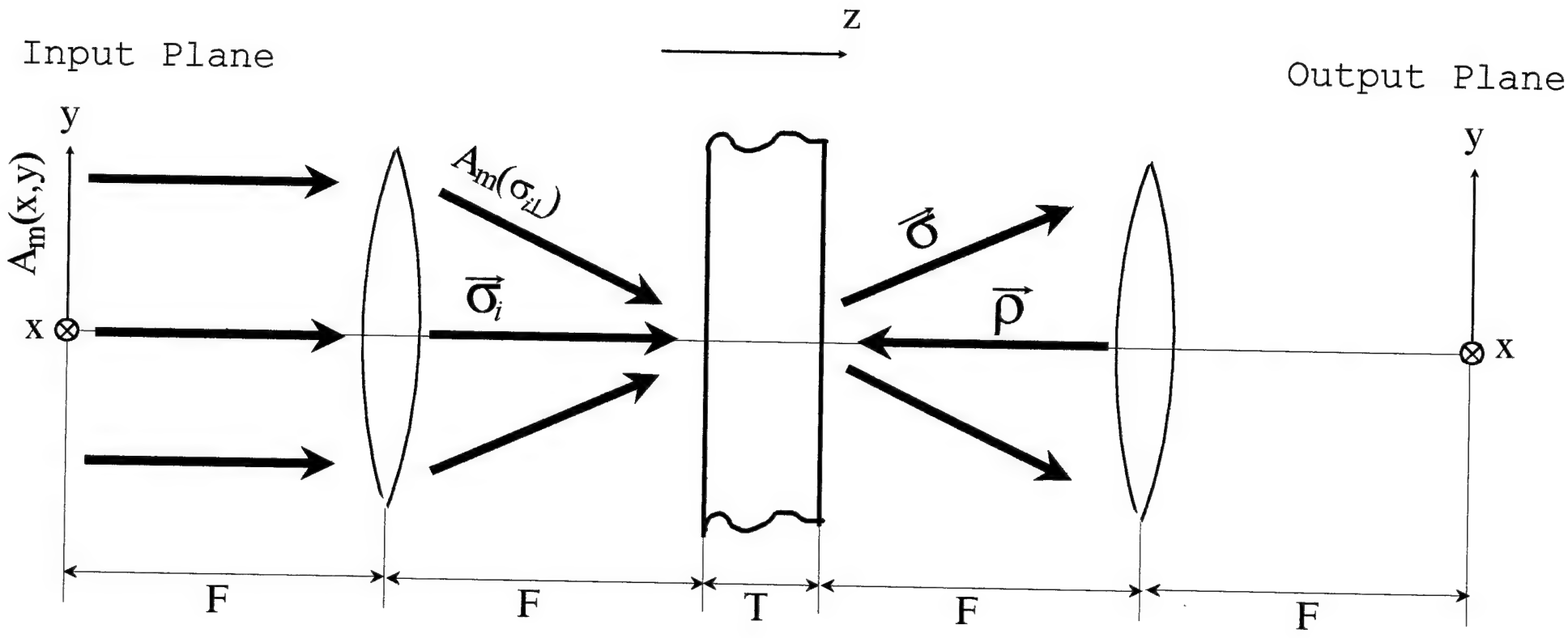


Fig.10 Recording and readout geometry for Fourier hologram storage [29].

written by interference of the wave $S_m(\vec{r})$ and oppositely traveling wave $R_m(\vec{r})$. These waves have the carrier wavelength $\lambda_{wm}$ and some spectrum $\delta\lambda$ around this wavelength. We label the gratings $m = 1,...M$. For the case when $\frac{\delta\lambda c}{\lambda_{wm}^2} << \frac{1}{\tau}$ ($\tau$ is the characteristic time of the recording and $c$ is speed of light) presence of these holograms modulates the permittivity of the material so that the change in the permittivity of the medium can be given by

$$\delta\hat{\varepsilon} \approx \alpha \sum_{m=1}^{M} R_m^*(\vec{r}) \cdot S_m(\vec{r}) + c.c. \tag{20}$$

Here, $\alpha$ is an efficient multiplier which takes into account the sensitivity of the material and degree of light coherence [40]. To retrieve, say, page ($l$), we illuminate the hologram with the wave $R_l(\vec{r})$ having carrying wavelength $\lambda_{rl}$. To describe the wave propagation, we use the scalar Helmholtz equation of the form

$$\nabla^2 A(\vec{r}) + \hat{\varepsilon}(\vec{r})\mu \frac{\omega^2}{c^2} A(\vec{r}) = 0 \tag{21}$$

in which $\omega$ is the optical frequency, $c$ is the speed of light, $\hat{\varepsilon}(\vec{r}) = \hat{\varepsilon}_a + \delta\hat{\varepsilon}$ is the dielectric permittivity, and $\mu$ is the magnetic permeability. We consider isotropic and nonmagnetic material, so $\mu$=1.

Following the coupled-wave theory [30], we seek solutions to the equation in the form

$$A(\vec{r}) = R_l(\vec{r}) + S(\vec{r}) = \int \hat{R}_l(\vec{\rho},z)\exp(-i\vec{\rho}\vec{r})d^3\rho + \int \hat{S}(\vec{\sigma},z)\exp(-i\vec{\sigma}\vec{r})d^3\sigma \quad (22)$$

where the amplitudes of each constituent plane wave of the wave vector $\vec{\rho}$ or $\vec{\sigma}$ vary in the thickness direction ($z$). Here and further, we choose the signal and reference waves such that their polarization vectors coincide. For the slowly varying amplitude approximation, we arrive at [32]

$$\int \rho_z \frac{d\hat{R}_l(\vec{\rho},z)}{dz} e^{-i\vec{\rho}\vec{r}} d^3\rho + \int \sigma_z \frac{d\hat{S}(\vec{\sigma},z)}{dz} e^{-i\vec{\sigma}\vec{r}} d^3\sigma + i\int \Gamma(\vec{\sigma})\hat{S}(\vec{\sigma},z)e^{-i\vec{\sigma}\vec{r}} d^3\sigma + \quad (23)$$
$$+i\int \chi(\vec{K})e^{-i\vec{K}\vec{r}} d^3K \int \hat{R}_l(\vec{\rho},z)e^{-i\vec{\rho}\vec{r}} d^3\rho + i\int \chi(\vec{K})e^{-i\vec{K}\vec{r}} d^3K \int \hat{S}(\vec{\sigma},z)e^{-i\vec{\sigma}\vec{r}} d^3\sigma = 0$$

Here $\Gamma(\vec{\sigma}) = \frac{\beta^2 - \sigma^2}{2}$; $\beta = \rho = \frac{2\pi}{\lambda_{rl}}\sqrt{\hat{\varepsilon}_a} = \frac{2\pi}{\lambda_{rl}} n_a$; $\sigma = |\vec{\sigma}|$; $\rho = |\vec{\rho}|$; and

$$\chi(\vec{K}) = \sum_{m=1}^{M} \frac{\alpha\beta^2}{\sqrt{\hat{\varepsilon}_a}} \int \hat{R}_m^*(\vec{\sigma}_i - \vec{K})\hat{S}_m(\vec{\sigma}_i)d^3\sigma_i \quad (24)$$

We neglect the intrasignal contribution $\hat{R}_m^*(\vec{\sigma}_i - \vec{K})\hat{R}_m(\vec{\sigma}_i)$ and $\hat{S}_m^*(\vec{\sigma}_i - \vec{K})\hat{S}_m(\vec{\sigma}_i)$ and the medium response dispersion.

The last terms of Eq.(23) can be rewritten as

$$I_4 = i\int \chi(\vec{K})e^{-i\vec{K}\vec{r}} d^3K \int \hat{R}_l(\vec{\rho},z)e^{-i\vec{\rho}\vec{r}} d^3\rho = i\iint \chi(\vec{K}'-\vec{\rho})\hat{R}_l(\vec{\rho},z)d^3\rho \cdot e^{-i\vec{K}'\vec{r}} d^3K' \quad (25)$$

$$I_5 = i\int \chi(\vec{K})e^{-i\vec{K}\vec{r}} d^3K \int \hat{S}(\vec{\sigma},z)e^{-i\vec{\sigma}\vec{r}} d^3\sigma = i\iint \chi(\vec{K}''-\vec{\sigma})\hat{S}(\vec{\sigma},z)d^3\sigma \cdot e^{-i\vec{K}''\vec{r}} d^3K'' \quad (26)$$

Since the wave $\hat{S}(\vec{\sigma},z)$ is the result of diffraction of $\hat{R}_l(\vec{\rho},z)$, the collections of wave vectors $\{\vec{K}'\}$ and $\{\vec{\sigma}\}$ coincide. Eq.(26) is presented as

$$I_5 = i \lim_{V_\rho \to 0} \left\{ \int_{V_\rho} e^{-i\vec{K}''\vec{r}} \int \chi(\vec{K}'' - \vec{\sigma}) \hat{S}(\vec{\sigma}, z) d^3\sigma \cdot d^3K'' + \int_{V - V_\rho} e^{-i\vec{K}''\vec{r}} \int \chi(\vec{K}'' - \vec{\sigma}) \hat{S}(\vec{\sigma}, z) d^3\sigma \cdot d^3K'' \right\} \quad (27)$$

where $V_\rho$ is the environs of point $\rho$ in the reciprocal space and $V - V_\rho$ is all the reciprocal space without $V_\rho$. The integral over $V - V_\rho$ is equal to zero because we can neglect the intermodulation terms and higher-order diffracted terms for Bragg diffraction and low diffraction efficiency. Therefore, the terms $I_1$ and $I_5$ in Eq.(23) describe the waves with wave vectors $\vec{\rho}$ and the terms $I_2$ and $I_4$ describe the waves with wave vectors $\vec{\sigma}$. So we obtain a system of equations similar to that given in Ref.[32].

$$\int \sigma_z \frac{d\hat{S}(\vec{\sigma}, z)}{dz} e^{-i\vec{\sigma}\vec{r}} d^3\sigma = -i \int \Gamma(\vec{\sigma}) \hat{S}(\vec{\sigma}, z) e^{-i\vec{\sigma}\vec{r}} d^3\sigma - i \iint \chi(\vec{\sigma} - \vec{\rho}) \hat{R}_l(\vec{\rho}, z) d^3\rho \cdot e^{-i\vec{K}'\vec{r}} d^3\sigma \quad (28a)$$

$$\int \rho_z \frac{d\hat{R}_l(\vec{\rho}, z)}{dz} e^{-i\vec{\rho}\vec{r}} d^3\rho = -i \lim_{V_\rho \to 0} \left\{ \int_{V_\rho} e^{-i\vec{K}''\vec{r}} \int \chi(\vec{K}'' - \vec{\sigma}) \hat{S}(\vec{\sigma}, z) d^3\sigma \cdot d^3K'' \right\} \quad (28b)$$

If the function under integral on the right-hand side of (28b) is limited, the left-hand side equals to zero, which corresponds to the Born approximation ($\frac{d\hat{R}_l(\vec{\rho}, z)}{dz} = 0$) that is valid for low diffraction efficiencies. Since the equations (28) are linear, one can change the sequence operations of summation and integration, and therefore (28a) transforms into

$$\frac{d\hat{S}(\vec{\sigma},z)}{dz} = -i\frac{\rho^2-\sigma^2}{2\sigma_z}\hat{S}(\vec{\sigma},z) - i\frac{\alpha\rho^2}{n_a\sigma_z}\sum_m\left[\hat{S}_m * \left(\hat{R}_m \bigstar \hat{R}_l\right)\right](\vec{\sigma}) \tag{29}$$

where the symbols * and ★ indicate convolution and correlation, respectively.

$$\left(\hat{R}_m \bigstar \hat{R}_l\right)(\vec{\sigma}) = \int \hat{R}_m^*(\vec{\sigma}'-\vec{\sigma})\hat{R}_l(\vec{\sigma}')d^3\sigma'$$

$$\left(\hat{S}_m * f\right)(\vec{\sigma}) = \int \hat{S}_m(\vec{\sigma}-\vec{\sigma}')f(\vec{\sigma}')d^3\sigma'$$

We seek solution of Eq.(29) in the form

$$\hat{S}(\vec{\sigma},z) = \tilde{S}(\vec{\sigma},z)exp\left(-i\frac{\Gamma(\vec{\sigma})}{\sigma_z}z\right) \tag{30}$$

Then Eq.(29) becomes

$$\frac{d\tilde{S}(\vec{\sigma},z)}{dz} = -i\frac{\alpha\rho^2}{n_a\sigma_z}\sum_m\left[\hat{S}_m * \left(\hat{R}_m \bigstar \hat{R}_l\right)\right](\vec{\sigma})\cdot exp\left(i\frac{\Gamma(\vec{\sigma})}{\sigma_z}z\right) \tag{31}$$

So the expression for the spectral amplitude of the output signal is

$$\hat{S}(\vec{\sigma},T) = -i\frac{\alpha\rho^2 T}{n_a\sigma_z}exp\left(-i\xi_r(\vec{\sigma},T)\right)sin\,c\left(\xi_r(\vec{\sigma},T)\right)\sum_m\left[\hat{S}_m * \left(\hat{R}_m \bigstar \hat{R}_l\right)\right](\vec{\sigma}) \tag{32}$$

where $\xi_r(\vec{\sigma},T)$ is the Bragg mismatch parameter [30]

$$\xi_r(\vec{\sigma},T) = \frac{\rho^2-\sigma^2}{4\sigma_z}T \tag{33}$$

For the Fourier transform storage by counterpropagating waves, we may represent the recorded data as

$$\hat{S}_m(\vec{\sigma}_i) = \hat{A}_m(\sigma_{i\perp})\bar{S}_m(\sigma_{iz})$$
$$\hat{R}_m(\vec{\rho}) = \delta(\rho_\perp)\delta(\rho_z + \rho)\hat{R}_m(\rho) \qquad (34)$$
$$\hat{R}_l(\vec{\rho}) = \delta(\rho_\perp)\delta(\rho_z + \rho)\hat{R}_l(\rho)$$

Here, $\hat{A}_m(\sigma_{i\perp})$ is related to a pixel at the point with coordinates $x$ and $y$ in the input plan through

$$\hat{A}_m(\sigma_{i\perp}) \sim A_m(x,y)\delta\left(\sigma_{ix} + \frac{\sigma_i}{n_a F}x\right)\delta\left(\sigma_{iy} + \frac{\sigma_i}{n_a F}y\right)$$
$$\bar{S}_m(\sigma_{iz}) \sim \delta\left(\sigma_{iz} - \sigma_i + \frac{1}{2}\sigma_i\left[\left(\frac{x}{n_a F}\right)^2 + \left(\frac{y}{n_a F}\right)^2\right]\right)S_m(\sigma_i) \qquad (34a)$$

For the reconstructed signal waves emerging from the medium the tangential components of the wave vector inside and outside the holographic medium are preserved at the boundary. However the length of the wave vector becomes $n_a$ times smaller. The amplitude of a constituent wave emerging from the medium therefore consists of the integral over all constituent waves corresponding to the same tangential components of the wave vector. This is expressed by [5]

$$\int \hat{S}(\vec{\sigma}, z)\exp(-i\sigma_z T)d\sigma_z = \bar{S}(\sigma_\perp, T) \qquad (35)$$

The intensity spectrum of the desired reconstructed hologram is

$$\left|\bar{S}^l(\sigma_\perp, T)\right|^2 =$$
$$= \left|\int \frac{\alpha\rho^2 T}{n_a\sigma_z}\hat{A}_l(\sigma_{i\perp})\exp\left(-i\xi_r(\vec{\sigma}, T)\right)\sin c\left(\xi_r(\vec{\sigma}, T)\right)\left[\bar{S}_l * \left(\hat{R}_l \bigstar \hat{R}_l\right)\right](\sigma_z)\exp\left[-i\sigma_z T\right]d\sigma_z\right|^2 \qquad (36)$$

and the intensity spectrum of the cross-talk is

$$\left|\hat{S}^N(\sigma_\perp,T)\right|^2 = \left|\bar{S}(\sigma_\perp,T)\right|^2 - \left|\bar{S}^l(\sigma_{i\perp},T)\right|^2 \qquad (37)$$

$$\left|\bar{S}(\sigma_\perp,T)\right|^2 =$$

$$= \left|\int \frac{\alpha\rho^2 T}{n_a\sigma_z} exp\left(-i\xi_r(\vec{\sigma},T)\right) sinc\left(\xi_r(\vec{\sigma},T)\right) \sum_{m\neq l} \hat{A}_m(\sigma_{i\perp}) \left[\bar{S}_m * \left(\hat{R}_m \bigstar \hat{R}_l\right)\right](\sigma_z) exp\left[-i\sigma_z(T)\right] d\sigma_z \right|^2 \qquad (38)$$

Following [5,29], we define the *NSR* as

$$NSR = \left\langle \frac{\left|\hat{S}^N(\sigma_\perp,T)\right|^2}{\left|\hat{S}^l(\sigma_\perp,T)\right|^2} \right\rangle \qquad (39)$$

where other noise sources are negligible and in which < > denotes the ensemble average.

Let us consider a particular case when holograms are recorded by ideally coherent plane waves, i.e., sinusoidal volume gratings are written, but reconstruction is carried out by the waves with the rectangular spectrum. The equivalent representation in the reciprocal space is

$$\begin{aligned} \hat{S}_m(\vec{\sigma}_i) &= A_{m0}\delta^2(\sigma_\perp)\delta(\sigma_{iz} - \beta^{(m)}) \\ \hat{R}_m(\vec{\rho}) &= R_{m0}\delta^2(\rho_\perp)\delta(\rho_z + \beta^{(m)}) \\ \beta^{(m)} &= \frac{2\pi}{\lambda_{wm}} n_a \end{aligned} \qquad (40)$$

To retrieve information, we illuminate the hologram with the wave $R_l(\vec{r})$

$$\hat{R}_l(\vec{\rho}) = \begin{cases} \delta^2(\rho_\perp)\delta(\rho_z+\rho)\dfrac{R_{l0}}{\Delta\rho}; & \beta^{(l)} - \Delta\rho \le \rho_z \le \beta^{(l)} + \Delta\rho \\ 0; \quad \text{otherwise} \end{cases} \qquad (41)$$

$$\beta^{(l)} = \frac{2\pi}{\lambda_{rl}} n_a \quad ; \quad \Delta\rho = \frac{2\pi}{\lambda_{rl}} \frac{\delta\lambda}{\lambda_{rl}}$$

where $\lambda_{rl}$ is the carrying wavelength of the readout wave. Then from (32) and (33) we obtain the expression for the output signal

$$\hat{S}(\vec{\sigma},T)=i\alpha T\delta^2(\sigma_\perp)\delta(\sigma_z-\sigma)\sum_m\frac{\left(2\beta^{(m)}-\sigma\right)^2}{n_a\sigma_z}\frac{A_{m0}R_{m0}R_{l0}}{\Delta\rho}\exp\left(i\xi_r^{(ml)}(\vec{\sigma},T)\right)\operatorname{sinc}\left(\xi_r^{(ml)}(\vec{\sigma},T)\right)$$

$$\xi_r^{(ml)}(\vec{\sigma},T)=\frac{\left(2\beta^{(m)}-\sigma\right)^2-\sigma^2}{4\sigma_z}T$$

$$\sigma=2\beta^{(m)}-\beta^{(l)}-\delta\rho;\quad \delta\rho\in\left[-\Delta\rho;\Delta\rho\right] \tag{42}$$

Then

$$S(T)=i\frac{\alpha'}{\Delta\rho}\int_{-\Delta\rho}^{\Delta\rho}\sum_m A_{m0}\frac{\left(2\beta^{(m)}-\sigma_z\right)^2}{\sigma_z}\exp\left(-i\xi_r^{(ml)}(\vec{\sigma},T)\right)\operatorname{sinc}\left(\xi_r^{(ml)}(\vec{\sigma},T)\right)\exp\left(-i\sigma_z z\right)d\sigma_z$$

$$\xi_r^{(ml)}(\vec{\sigma},T)=\frac{\beta^{(m)}\left(\beta^{(m)}-\beta^{(l)}-\delta\rho\right)}{2\beta^{(m)}-\beta^{(l)}-\delta\rho}T \tag{43}$$

$$\alpha'=\frac{\alpha A_{m0}R_{m0}R_{l0}}{n_a}T;\quad \sigma_Z=2\beta^{(m)}-\beta^{(l)}-\delta\rho$$

This expression describes the amplitude of the reconstructed signal. It is worth noting that (43) is a particular case of Eq.(35), when only one pixel at $x=y=0$ has been recorded. However, actually this result describes a general case because, as it was shown in the preceding section, we can ignore cross-talk due to comlexity of the recording images.

Now we turn to numerical calculations of the cross-talk. We assume that the stored images $A_{m0}$ are independent random variables taking the value of zero and unity with equal propbability. In the wavelength multiplexing, the condition of uncorrelated phases is typically realized and in consequence the cross-talk terms in (39) add incoherently. Let the

recording wavelengths be separated from each other by the interval equal to the wavelength selectivity of the medium.

The *NSR* for the hologram stored at the center wavelength ($\lambda_{wM/2}$) was obtained by numerically calculating the dependences (42) and (39) for $T = 1$ cm, $\lambda_{w1} = 0.5\mu$m and $M > 10$ Fig.11 shows the dependence of *NSR* on the relative width ($\delta\lambda/\Delta\lambda_0$) of the readout light spectrum. The cross-talk rapidly increases with increasinng spectrum width, and at $\delta\lambda = 0.8\,\mathring{A}$ *NSR* is greater than 0.1. Thus the wavelength multiplexing requires a light source with high coherence, two - three times higher than the wavelength selectivity of the medium.

Fig.12 shows *NSR* as a function of hologram number. Fig.13 presents *NSR* versus the quantity of stored holograms (pages). Note that *NSR* for the first and the last hologram ($l = 0$ and $l = M$) is twice as low as that for the holograms in the middle position. This is because the holograms in the extreme positions have neighbors only from one side. Therefore, the maximum *NSR* is always observed for the middle hologram in the schedule. Moreover, as one can see from Figs.12,13, *NSR* is determined by the amount of holograms which have overlap with the readout light spectrum. In our case ($\delta\lambda/\Delta\lambda_0 < 2$) only the nearest neighbors give contribution to the cross-talk, and for the holograms in the middle position *NSR* is nearly independent of the amount of holograms.

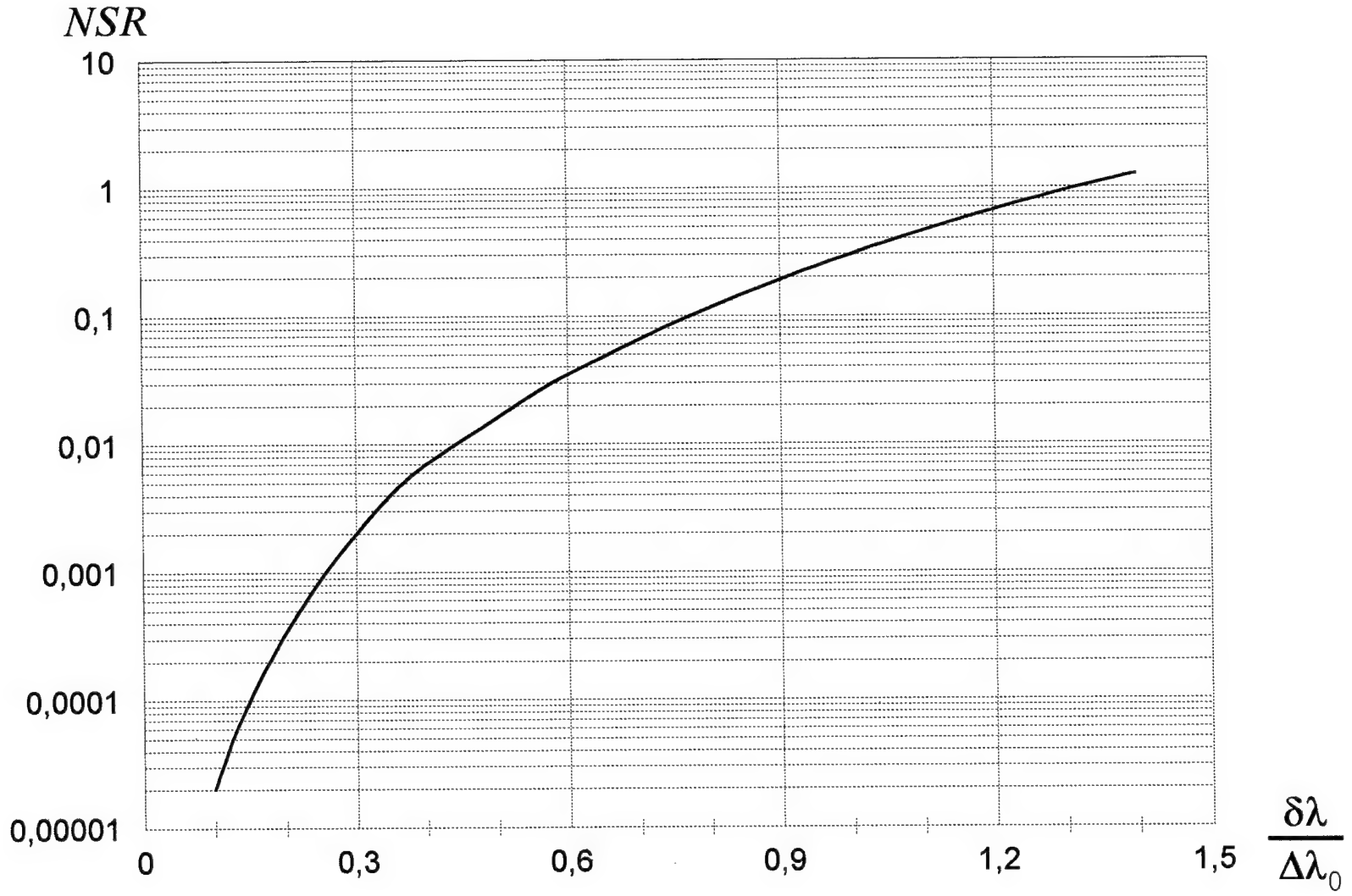


Fig.11 *NSR* versus the relative width of the readout light.

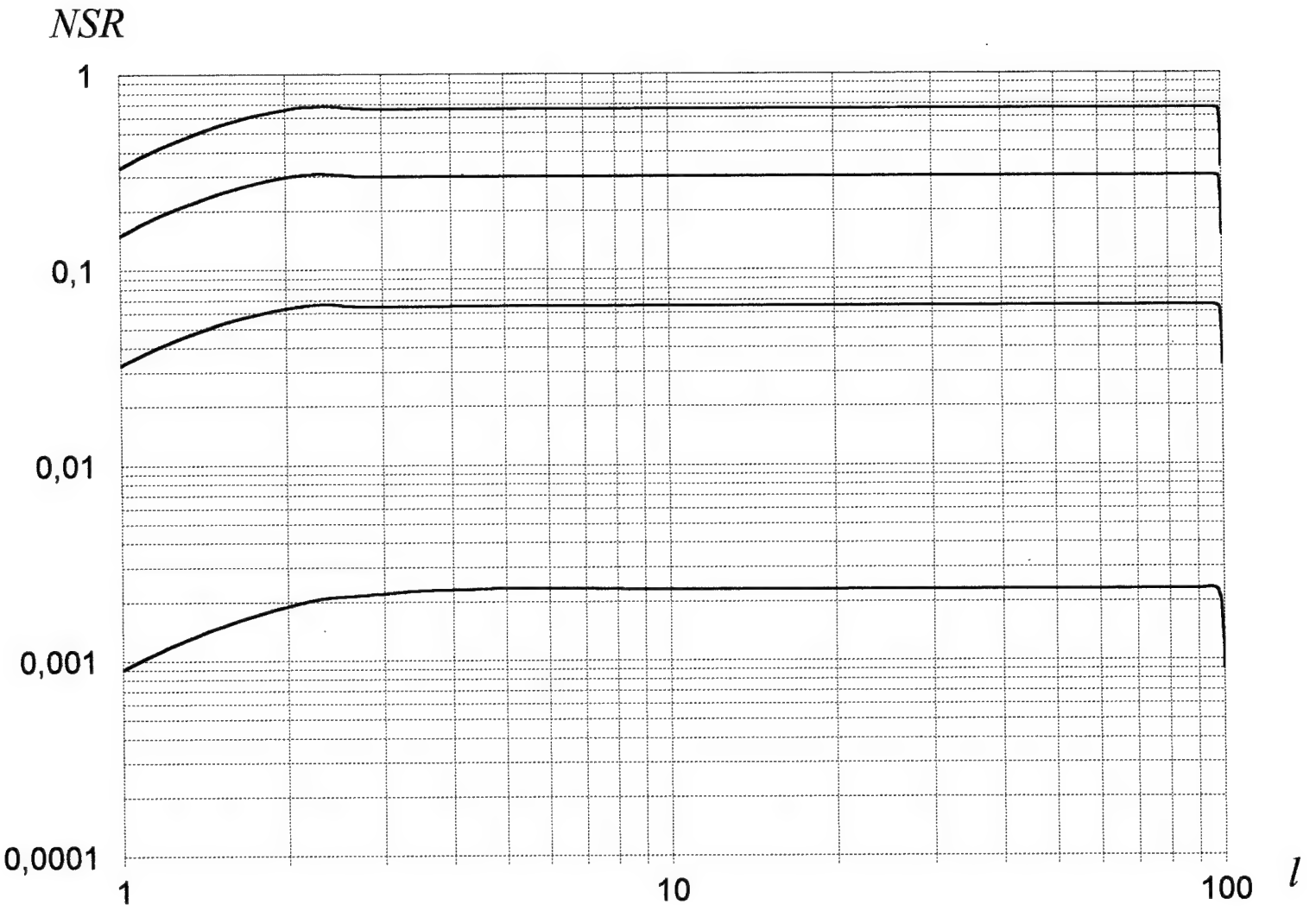


Fig.12 *NSR* as a function of the hologram number for several width of the readout light spectrum ($\delta\lambda/\Delta\lambda_0$). (1) - 0.3; (2) - 0.7; (3) - 1; (4) - 1.2.

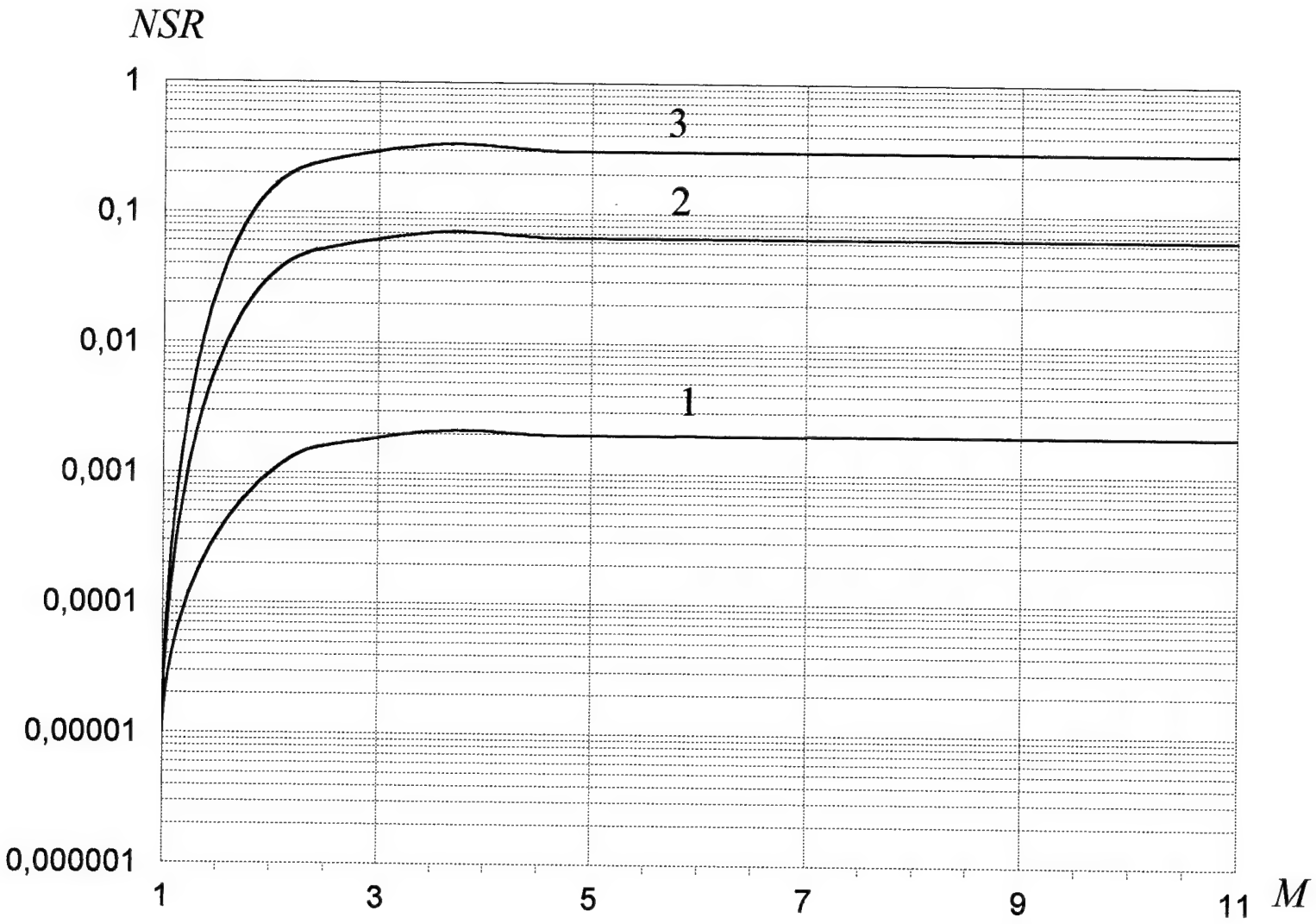


Fig.13 *NSR* as a function of the total number of hologram for several width of the readout light spectrum ($\delta\lambda/\Delta\lambda_0$). (1) - 0.3; (2) - 0.7; (3) - 1.

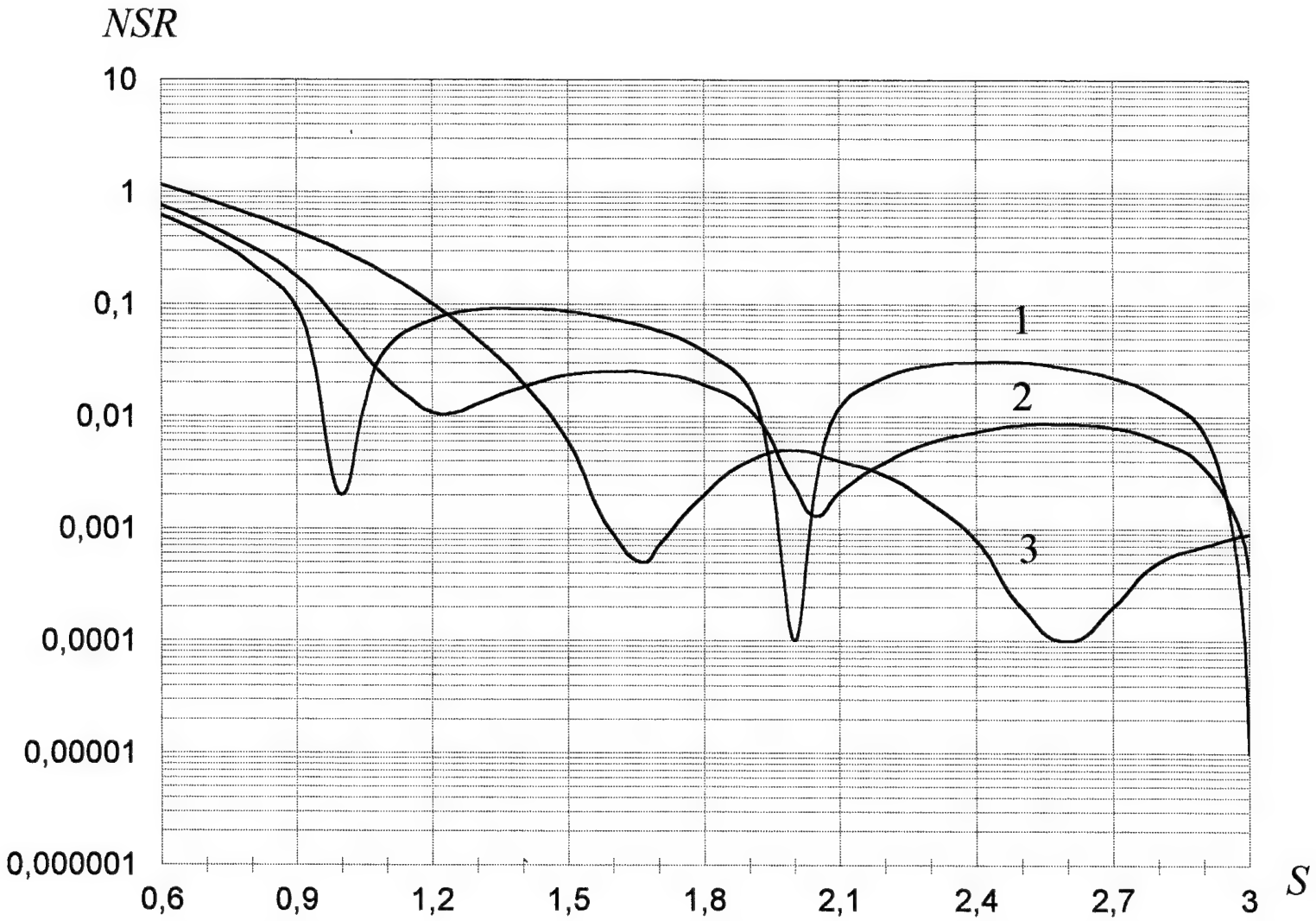


Fig.14 *NSR* as a function of the sparseness of reference wavelegth selection for several width of the readout light spectrum($\delta\lambda/\Delta\lambda_0$). (1) - 0.3; (2) - 0.7; (3) - 1.

The sparse selection can lead to some improvements the the cross-talk performance [31]. $NSR$ as a function of sparseness ($S$) is plotted in Fig.14 for several values of $(\delta\lambda/\Delta\lambda_0)$. Note that, for very broad spectra, cross-talk if not locally minimized when $S$ is an integer as for coherent readout light.

To summarize, the main results described in this chapter are as follows:

1. Two sources of cross-talk have been analyzed. They are the cross-talk due to complicated structure of the recorded image and the cross-talk due to the limited coherence of the readout light.

2. The comprehensive mathematical analysis of the cross-talk due to the limited coherence of the readout light has been carried out and it has been shown that this factor can play a critical role in the wavelength multiplexing.

3. The numerical calculations of the dependences of cross-talk on the width of the readout light spectrum and on the quantity of recorded holograms have been performed. These data allow one to draw recommendations concerning the optimization of the hologram recording conditions for each particulat case. In the simplest situation, it is necessary to satisfy the following requirements:

- $\delta\lambda/\Delta\lambda_0 < 1/3$; and
- the accuracy of the wavelength positioning should be better than $\Delta\lambda_0$.

The refractive index variations are equivalent from the point of view of maximum selectivity to variations in $\Delta\lambda$ [33]. So the maximum electric field selectivity is reached in the reflection geometry of volume holograms. The first papers concerned with the electric field control of volume holograms in $LiNbO_3$ in the reflection geometry were published in 1978-1979 [37,38,39]. By these experiments, the electric field multiplexing was demonstrated and six holograms could be reconstructed separately by varying the electric field. More recently the interest to this effect arose again. This was associated with the progress in development of the volume holographic memory [2] and with a wider use of holographic materials for high-selectivity holographic filters [36].

The theory of electric field selectivity has been described in detail in the Interim Report. So here we shall remind briefly the main results of calculations and more attention will be paid to the experimental data.

Following [30], one can calculate the diffraction efficiency for the volume reflection hologram as a function of the refractive index variations. It results in the formula similar to Eq.(4), where the term $\xi_r$ is replaced by $\xi_r^e$

$$\xi_r^e = \beta T \frac{\Delta n_a}{n_a} sin\theta_0 \qquad (44)$$

For the photorefractive materials, variations in $\Delta n_a$ mean variations in the ordinary or extraordinary refractive index

under the applied electric field. So variations in $\Delta n_a$ due to electric field result in violation of the Bragg condition and destruction of diffraction. That is why the hologram must be read out the same magnitude of electric field at which recording takes place. However, variations in the electric field result not only in variations in the refractive index but also in the sample deformation. This happens because an electrooptic crystal exhibits the piezoelectric effect. Then it follows from the Bragg condition that the diffraction efficiency goes to zero when [33,34]

$$\frac{dK_g}{dn_a}\Delta n_a + \frac{dK_g}{d\Lambda}\Delta\Lambda = \frac{2\pi}{T}$$
$$\text{or} \qquad \frac{\Delta n_a}{n_a} + \frac{\Delta\Lambda}{\Lambda} = \frac{\Lambda}{T} \tag{45}$$

Here, $\Delta\Lambda$ is the change in the grating spacing due to the sample deformation. The physical meaning of this relationship is very clear. The change in the optical path $T\cdot\Delta n_a + n_a\Delta T$ must be equal to $\lambda/2$. Let us remind that if we ignore deformation of the sample, then $\frac{\Delta n_a}{n_a} = \frac{\Lambda}{T}$. This relationship follows immediately from the condition $\xi_r^e = \pi$, and it was also derived in the Interim Report from the simple Fourier analysis of the grating having a limited thickness. The numerical estimations of the magnitude of $\Delta\Lambda$ under sample deformation caused by the piezoelectric effect can be made if the necessary values of the piezolectric coefficients ($d_{ikl}$) are known since $\Delta\Lambda/\Lambda = d_{ikl}E_i$ [34,35]. They are available for $LiNbO_3$.

Evaluation shows that for definite orientations of the crystal the magnitude of $\Delta\Lambda/\Lambda$ can be of the order of $10\div30\%$ of $\Delta n_a / n_a$. So these deformations play a minor role compared to the electrooptic effect. Very often, from the experimental point of view, there is no reason to separate these two contributions because the sample deformation can be taken into account in the expression for the holographic selectivity by renormalizing the electrooptic coefficients. In our particular case, when we compare the theoretical calculations (see the text below) with the experimental data, an excellent agreement between the theory and experiment was obtained when we used the literature data on the electrooptic coefficients. That means that in our case we can ignore the piezoelectric effect.

In photorefractive materials, there can be a contradiction between the requirement of high electric field selectivity of a hologram and high diffraction efficiency because of the anisotropy of the material. So we should look for a compromise between these conflicting requirements. Let us consider some examples. We select a definite geometry for recording holograms in $LiNbO_3$ when $\vec{E}\perp\vec{K}_g$, $\vec{K}_g$ being at $45^0$ to the $\vec{C}$ axis. We consider only the transverse electrooptic effect. In this case there is a possibility to reduce the applied voltage proportionally to the ratio $T/d$ (Fig.16). For this case

$$K_{gx}=0 \quad ; \quad K_{gy}=\frac{K_g}{\sqrt{2}} \quad ; \quad ;K_{gz}=\frac{K_g}{\sqrt{2}} \qquad (46)$$

$$\delta\hat{\varepsilon} = \frac{\delta D}{\left|\vec{K}_g\right|\sqrt{2}} \begin{vmatrix} \frac{r_{13}}{\varepsilon_{33}} n_0^4 & 0 & 0 \\ 0 & \frac{r_{13}}{\varepsilon_{33}} n_0^4 & \frac{r_{51} n_e^2 n_0^2}{\varepsilon_{11}} \\ 0 & \frac{r_{51} n_e^2 n_0^2}{\varepsilon_{11}} & \frac{r_{33}}{\varepsilon_{33}} n_e^4 \end{vmatrix} \qquad (47)$$

$$\vec{e}_0 = \begin{vmatrix} 1 \\ 0 \\ 0 \end{vmatrix} \qquad \vec{e}_e = \begin{vmatrix} 0 \\ -\frac{1}{\sqrt{2}} \\ \frac{1}{\sqrt{2}} \end{vmatrix} \qquad (48)$$

Here, $r_{ij}$ are the electrooptic coefficients, $\varepsilon_{ij}$ is the dielectric tensor ($\varepsilon_{11}=\varepsilon_{22}=78$ and $\varepsilon_{33}=32$ for $LiNbO_3$), and $\delta D$ is the space charge grating amplitude which is formed under holographic recording. Here and later we omit the multiplier $4\pi$ in the dependence of $\vec{E}_g$ on $\delta D$. $\vec{e}_0$ and $\vec{e}_e$ are unit vectors for the ordinary and extraordinary polarizations.

Then for readout by the ordinary beam $\vec{e}_\rho = \vec{e}_\sigma = \vec{e}_0$

$$\left\langle \vec{e}_0 \delta\hat{\varepsilon} \vec{e}_0 \right\rangle = \frac{\delta D}{\sqrt{2}\left|\vec{K}_g\right|} \frac{r_{13}}{\varepsilon_{33}} n_0^4 \qquad (49)$$

and the diffraction efficiency for the ordinary beam in the absence of the external field is

$$\eta = \frac{1}{cth^2\left[\frac{\pi}{\lambda}\frac{\delta D}{\sqrt{2}\left|\vec{K}_g\right|}\frac{r_{13}}{\varepsilon_{33}}\frac{n_0^3}{2\sin\theta_0}\right]} = \frac{1}{cth^2\left[E_{gz}\frac{\pi}{\lambda}\frac{r_{13} n_0^3}{2\sin\theta_0}\right]} \qquad (50)$$

where

$$E_{gz} = \frac{\delta D}{\sqrt{2}\varepsilon_{33}\left|\vec{K}_g\right|} \tag{51}$$

For the readout by the extraordinary beam $\vec{e}_\rho = \vec{e}_\sigma = \vec{e}_e$

$$\left\langle \vec{e}_e \delta\hat{\varepsilon}\vec{e}_e \right\rangle = \frac{\delta D}{2\sqrt{2}\left|\vec{K}_g\right|}\left(\frac{r_{13}n_0^4}{\varepsilon_{33}} + \frac{r_{33}n_e^4}{\varepsilon_{33}} - 2\frac{r_{51}n_0^2 n_e^2}{\varepsilon_{11}}\right) \tag{52}$$

and the diffraction efficiency (again with $E = 0$) is

$$\eta = \frac{1}{cth^2\left[\frac{\pi}{\lambda}\frac{E_{gz}}{2n_e \sin\theta_0}\left(\frac{r_{13}n_0^4}{\varepsilon_{33}} + \frac{r_{33}n_e^4}{\varepsilon_{33}} - 2\frac{r_{51}n_0^2 n_e^2}{\varepsilon_{11}}\right)\right]} \tag{53}$$

Since the ratio $\left\langle \vec{e}_0 \delta\hat{\varepsilon}\vec{e}_0 \right\rangle \Big/ \left\langle \vec{e}_e \delta\hat{\varepsilon}\vec{e}_e \right\rangle \approx 1.28$, the ratio $\eta_0/\eta_e$ is of the order of 1.6.

Then we consider the influence of the external electric field $\vec{E}$. In accordance with Fig.18, $E_x = 0$, $E_y = -\frac{\left|\vec{E}\right|}{\sqrt{2}}$, $E_z = \frac{\left|\vec{E}\right|}{\sqrt{2}}$, and the equation for the optical indicatrix is

$$\left(\frac{1}{n_0^2} + r_{13}E_z\right)x^2 + \left(\frac{1}{n_0^2} + r_{13}E_z\right)y^2 + \left(\frac{1}{n_z^2} + r_{33}E_z\right)z^2 + 2yzr_{42}E_y = 1 \tag{54}$$

The plane which is normal to $\vec{\rho}$ is

$$K_{gy}y + K_{gz}z = 0$$
$$y = -z \tag{55}$$

Solution of (54) and (55) results in the relationships for the new magnitudes of $n_0$ and $n_e$., i.e., $n_{0h}$ and $n_{eh}$. They are

$$n_{0h} = n_0 - \frac{1}{2}n_0^{\,3}r_{13}\frac{E}{\sqrt{2}}$$
$$\Delta n_0 = -\frac{1}{2}n_0^{\,3}r_{13}\frac{E}{\sqrt{2}} \tag{56}$$

$$n_{eh} = \frac{\sqrt{2}n_e n_0}{\sqrt{n_e^{\,2} + n_0^{\,2}}} - \left(\frac{n_e n_0}{\sqrt{n_e^{\,2} + n_0^{\,2}}}\right)^3 \left(r_{51} + \frac{r_{33}}{2} + \frac{r_{13}}{2}\right)E$$
$$\Delta n_e \approx \frac{n_e^{\,3}}{2\sqrt{2}}\left(r_{51} + \frac{r_{33}}{2} + \frac{r_{13}}{2}\right)E \tag{57}$$

It follows from (56) and (57) that the electric field affects much stronger the extraordinary refractive index than the ordinary refractive index because $\Delta n_e$ / $\Delta n_0$ ≈ 5.2. So the electric field selectivity will be higher for the extraordinary beam.

Since the refractive indices are changed by the external electric field $\vec{E}$, the value of $\xi_r^e$ in (44) is not equal to zero and the final expression for the diffraction efficiency $\eta_e$ will be

$$\eta_e = \frac{1}{\left(\xi_r^e / \nu_r^e\right)^2 + \left[1 - \left(\xi_r^e / \nu_r^e\right)^2\right] cth^2\left[\nu_r^{e\,2} - \xi_r^{e\,2}\right]^{\frac{1}{2}}} \qquad (58)$$

where

$$\xi_r^e = -\frac{\beta T n_e^{\,2}}{2\sqrt{2}}\left(r_{51} + \frac{r_{33}}{2} + \frac{r_{13}}{2}\right)E = \frac{\pi n_e^{\,3} T}{\sqrt{2}\lambda}\left(r_{51} + \frac{r_{33}}{2} + \frac{r_{13}}{2}\right)E$$

$$\nu_r^e = \frac{\pi}{\lambda}\frac{T}{\sin\theta_0}\frac{\delta D}{2\sqrt{2}\left|\vec{K}_g\right| n_e}\left(\frac{r_{13} n_0^{\,4}}{\varepsilon_{33}} + \frac{r_{33} n_e^{\,4}}{\varepsilon_{33}} - 2\frac{r_{51} n_0^{\,2} n_e^{\,2}}{\varepsilon_{11}}\right)$$

Expression of this type can also be written for $\eta_0$. However, since electric field selectivity is higher for the extraordinarily polarized beam, we shall not analyze $\eta_0$.

For the experiments, $Fe^{2+}$-doped single crystals of $LiNbO_3$ were used. The concentration of $Fe^{2+}$ was less than 0.05% mol. The orientation shown in Fig.15 was chosen. The recording light beams illuminated the opposite surfaces of the crystal so that the angle between the optical $\vec{C}$ axis and the recorded hologram vector was $45^0$. The sample size $T$ along the light propagation direction was 1 cm, the height $d$ was 3.3mm. Electrodes were deposited on the upper and lower surfaces by a conducting silver paint.

The optical part of the setup depicted in Fig.16 was a conventional holographic scheme used for recording of reflection holograms.

Fig.17 shows the comparison between the experimental and theoretical dependences of diffraction efficiency on the

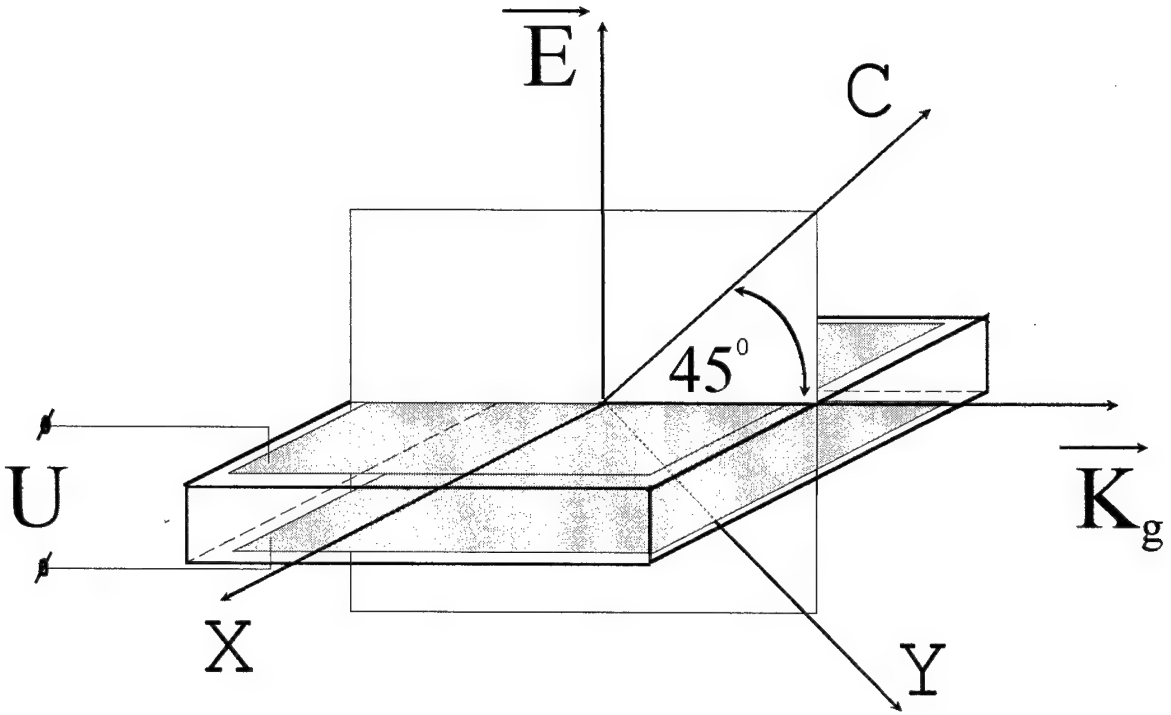


Fig.15 Orientation of the $LiNbO_3$ crystal used in the experiments on investigation of electric field multiplexing.

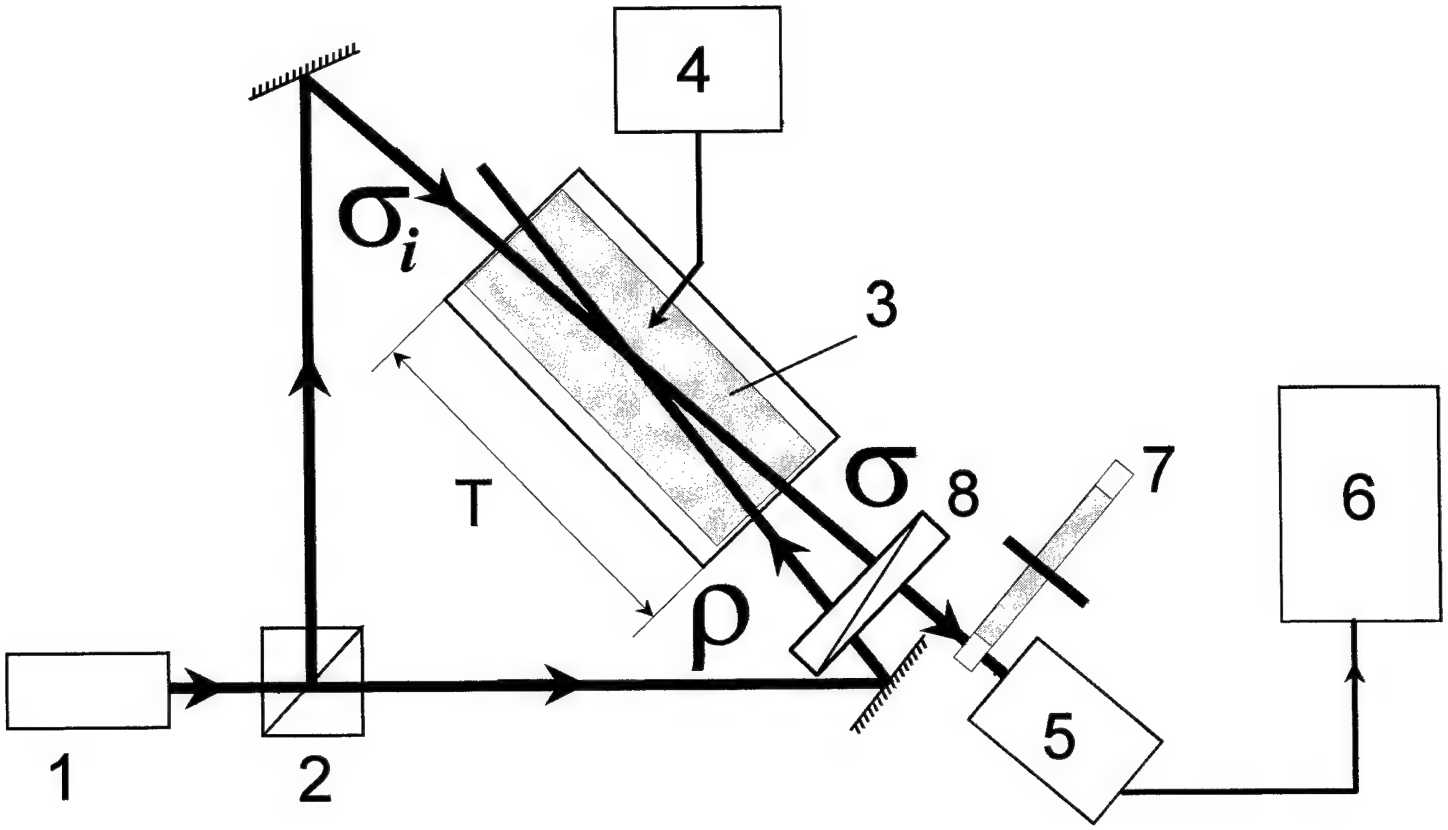


Fig.16 Experimental setup for the investigations of electric field multiplexing. (1) - a He-Ne laser, (2) - a beamsplitter, (3) - a $LiNbO_3$ crystal with the upper electrode, (4) - a high-voltage source, (5) - a photodetector, (6) - a lock-in amplifier, (7) - a shutter, (8) - a polarizer, $\rho$ and $\sigma_i$ are the wave vectors of recording beams, $\sigma$ is the wave vector of the reconstructing beam.

applied voltage for the ordinary and extraordinary polarizations. One can see that the selectivity is higher for the extraordinary polarization. This agrees with the theory because the ratio $\Delta n_e/\Delta n_0 \approx 5.2$.

Fig.18 shows diffraction efficiency as a function of electric field for two holograms recorded under different applied fields.

As one can see from Fig.17, in our experiments, at $\xi^e_r=\pi$, $\eta_e$ was of the order of $0.05\eta_{emax}$. However, according to the theory, $\eta_e$ at $\xi^e_r=\pi$ must go to zero. This difference between the theoretical and experimental values is caused by a "background signal". Several sources of the background signal can be mentioned. One of the main origins of the background signal is penetration of both eigenmodes (ordinary and extraordinary beams) through the input polarizer because, for different eigenmodes, the zeroes of diffraction efficiency correspond to different magnitudes of the external electric field. For instance, the background signal increases by a factor of 4.3 when a polarizer is removed. Another important source of the background signal is the inhomogeneity of the external electric field inside the crystal. To clarify the role of the electric field inhomogeneity, the experiments with different configurations of electrodes were carried out (Fig.19). The experiments have shown that a reduction in the dimensions of the upper electrode and, hence, an increase in the electric field inhomogeneity in the crystal results in a decrease in the electric field selectivity and increase in the background

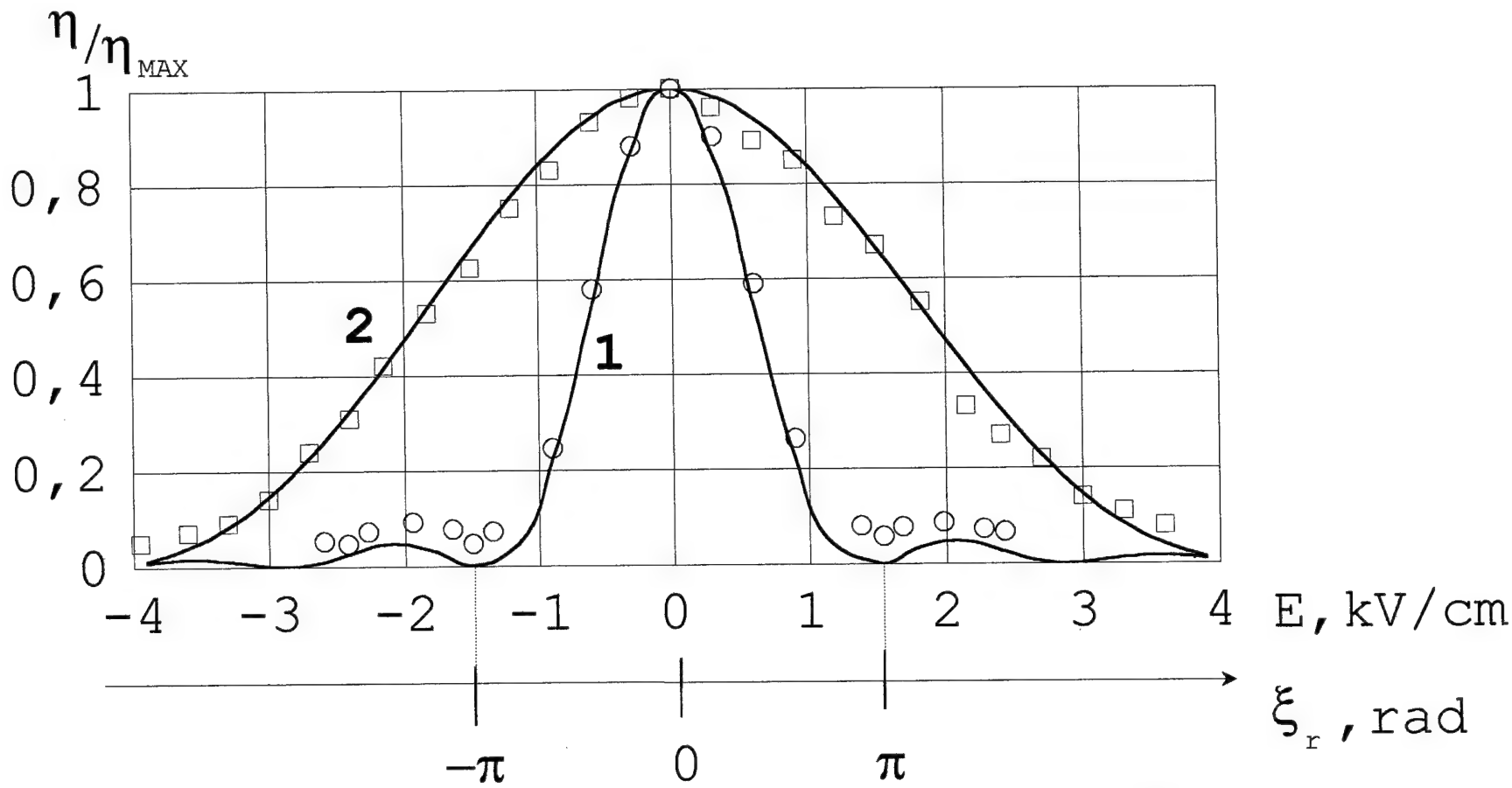


Fig.17 Comparison of the theoretical (solid curves) and experimental dependences of diffraction efficiency on the applied electric field (for $\eta_{max}<<1$). (1) - extraordinary polarization, (2) - ordinary polarization. The axis $\xi r$ is shown only for the extraordinary polarization. No fitting parameters were used.

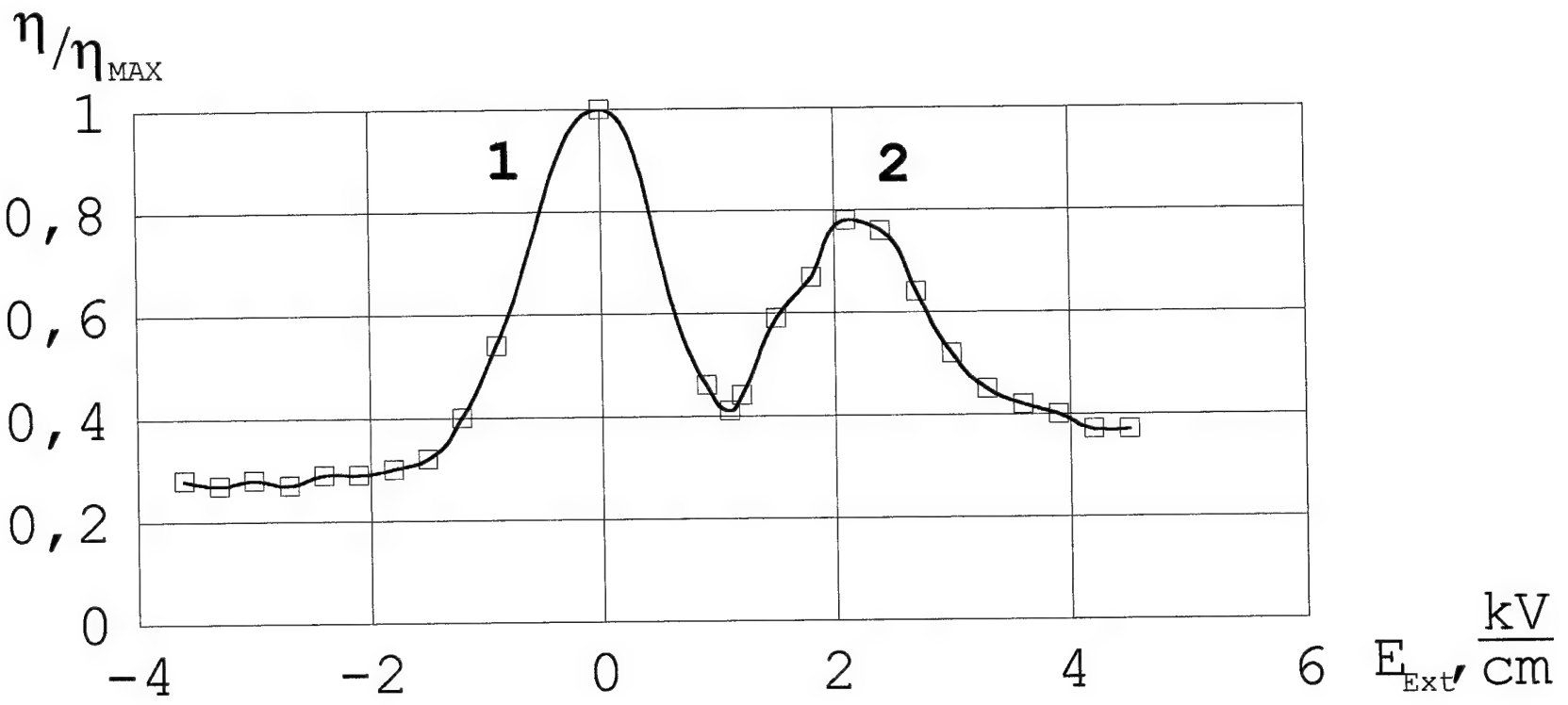


Fig.18 Diffraction efficiency as a function of applied electric field when two holograms were recorded in different electric fields. The solid curve is only for eye's help.

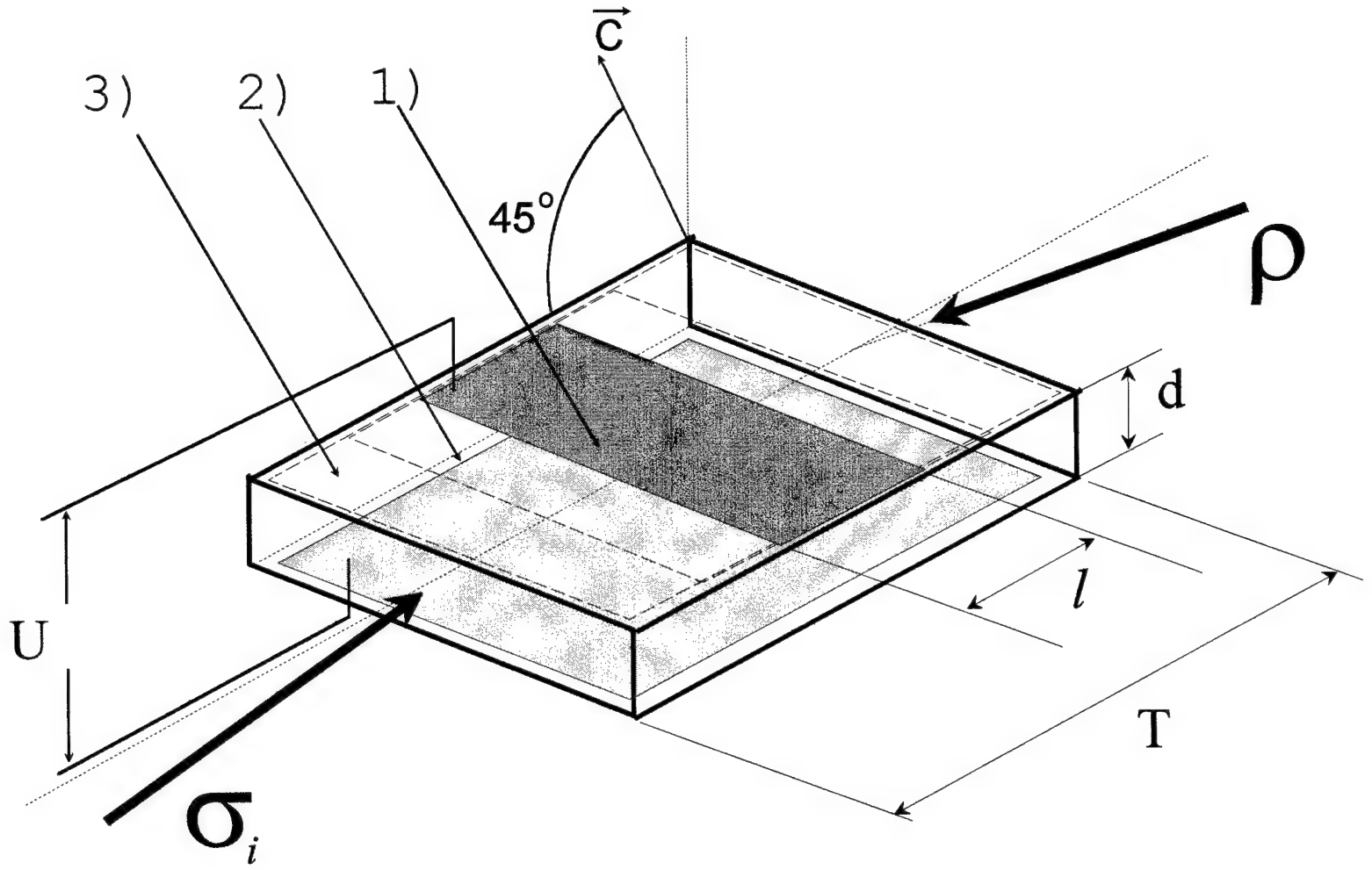


Fig.19 The crystal with different upper electrodes.
(1)- *l*=2mm; (2)- *l*=4mm; (3)- *l*=T

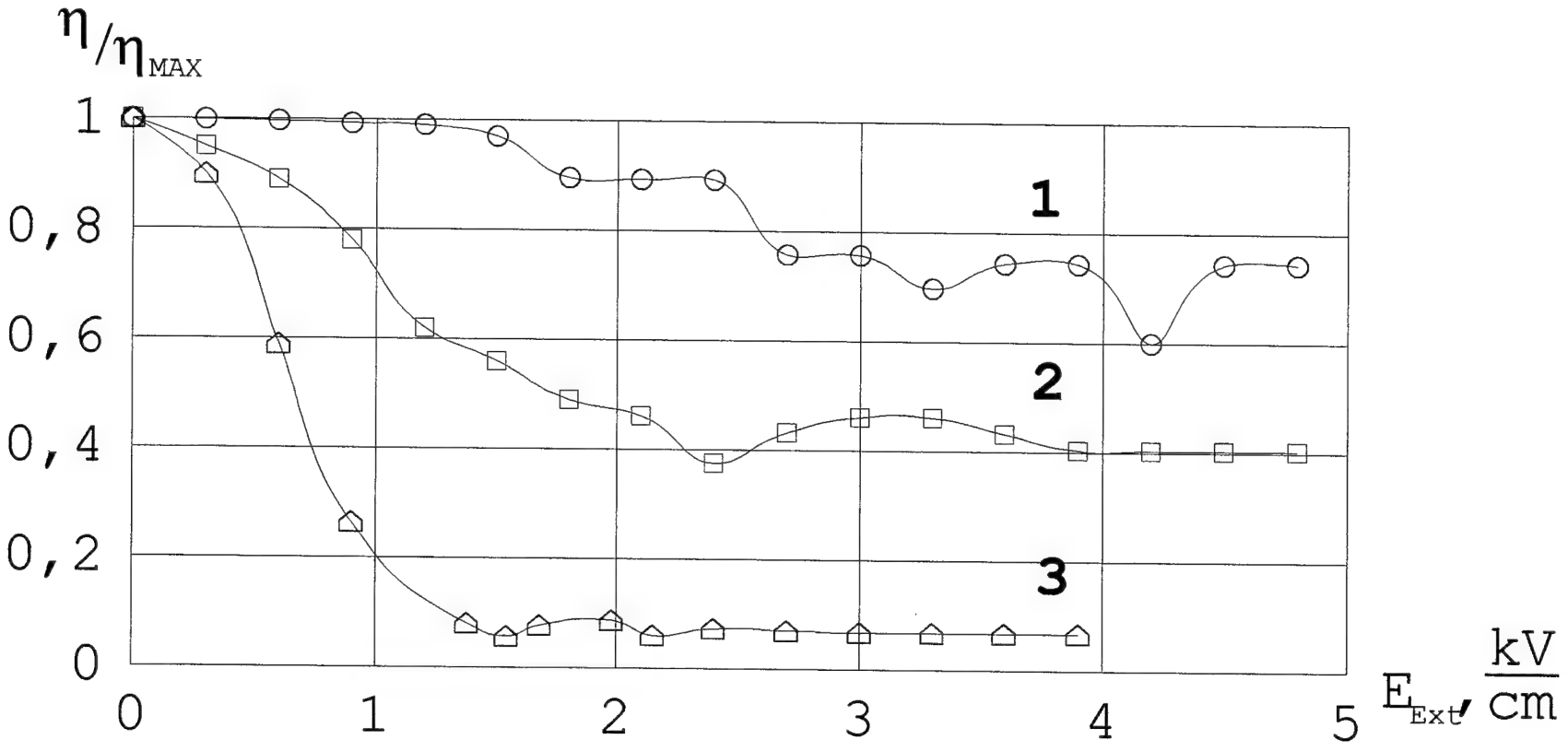


Fig.20 Diffraction efficiency as a function of applied electric field for electrodes with different sizes.

(1)- $l$=2mm; (2)- $l$=4mm; (3)- $l$=T

signal(Fig.20). Another way to create the electric field inhomogeneity in the crystal is to illuminate the crystal by a beam with a strongly inhomogeneous intensity across the cross section. Since the $LiNbO_3$ crystal is a photoconductor, the illumination inhomogeneity creates the internal electric field inhomogeneity and, in addition, results in the inhomogeneity of the sample temperature. Fig.22 shows the experimental data for various cross sectional areas of the readout beam (Fig.21). It is clearly seen that a high background signal and poor electric field selectivity correspond to readout by the beam with the cross sectional area smaller than the transverse dimensions $f$ of the sample.

From Fig.17 we can estimate the upper limit of the electric field multiplexing $M_{ef}$ as $M_{ef} = \eta_{max}/\eta_{\xi=\pi} \approx 10 \div 20$. On the other hand, to vary $\xi^e_r$ from 0 to $\pi$ one must apply the electric field $E$ equal to 1560 V/cm. Let us assume that the breakdown field in air is equal to $E_{bd} = 30$ kV/cm. In this case the upper limit of the electric field multiplexing can be estimated as $M'_{ef} = 2 \times 20$.

Factor "2" arises because one can use positive and negative electric fields. From the above discussion it can be concluded that the background signal is the main factor in our experiments which limits the magnitude of electric field multiplexing.

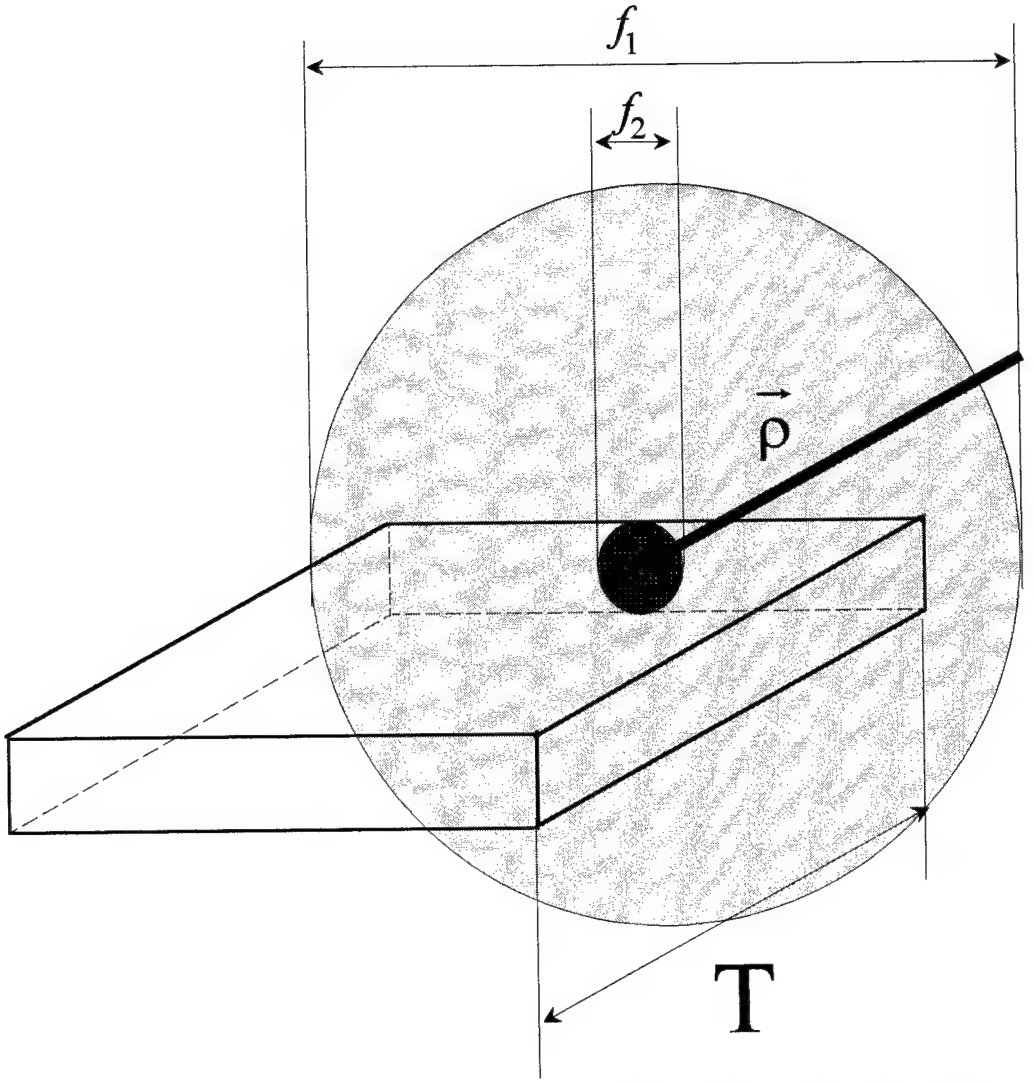


Fig.21 The readout by beams with various cross section areas.
(1)- $f_1$= 17 mm; (2)- $f_2$= 3 mm

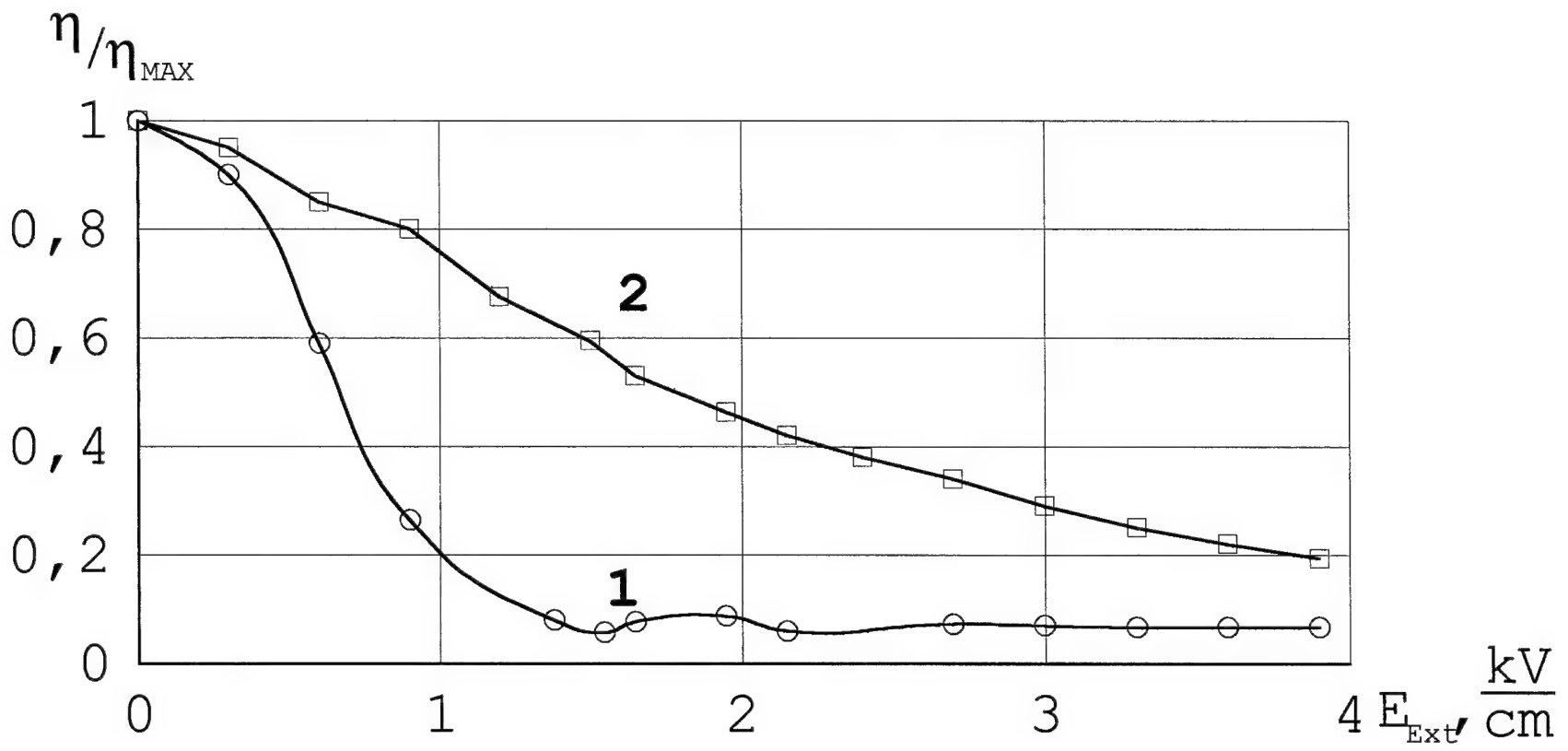


Fig.22 Diffraction efficiency as a function of applied electric field for different widths of recording beams.
(1)- 17mm; (2)- 3mm.

Thus, the obtained results are as follows:

1. A required setup for the experimental investigations of the electric field multiplexing has been built and properly cut, oriented, and polished single crystals of $LiNbO_3$ have been prepared.
2. An efficient configuration for recording reflection holograms which provides a high diffraction efficiency and efficient electric control has been found for $LiNbO_3$. The required theoretical calculations and experiments have been performed.
3. A theory for the electric field selectivity in photorefractive materials has been developed. The comparsion of theoretical calculations with the experimental data exibits an excellent agreement at the certain conditions.
4. The experiments have shown that the electric field inhomogeneity plays an important role in reduction of the electric field selectivity.
5. The investigations have shown that the electric field multiplexing of the order of 20 is realistic.

## *Chapter 4. Dynamic Range and Light Scattering from Volume Holograms*

The information capacity of one page of information can be estimated as [41]

$$4AW^2 \log_2\left(1+\frac{P_s}{P_n}W^2\right) \tag{59}$$

Here, $A$ is the area of the hologram, $W$ is the 1-D spatial frequency bandwidth of the hologram, and $P_s/P_n$ is the signal-to-noise power spectrum ratio. The important assumption is that the dependence of diffraction efficiency on spatial frequency is a constant over the interval of $W$. It should be emphasized that actually the bandwidth $W$ depends on noise [42,43]. This is due to the fact that the noise does not allow the use of a broader bandwidth when sensitivity of the material decreases with increasing spatial frequency. So $W$ is an efficient noise-dependent parameter.

The definition of $P_s$ requires some comments. In (59), $P_s$ means the noise power spectrum taken for all spatial frequencies over the area $W^2$. So to find the experimental value of $P_s/P_n$, it is necessary to record the noise-like image whose spectrum is spread over the entire area $W$ x $W$ of spatial frequencies. This differs appreciably from the measurement technique involving recording of only one grating

and estimation of $P_s/P_n$ from it [44]. In the last case the ratio $P_s/P_n$ is measured for the "narrow-band" configuration. The difference between the data on $P_s/P_n$ obtained by the two techniques can be as high as many orders of magnitude, so one has to be very careful in using the data obtained from the narrow-band measurements for estimating the information capacity of the hologram.

There are several sources of noise. In real practical systems one has to take into account the noises caused by the scattered light from the photosensitive media where holograms are recorded, the photon-shot noise resulting from the limited photon flux in the weak recording beam [44], and the photoreceiver noise. The scattered light can have several main sources. They are the cross-talk, optical scattering due to a poor quality of the crystal surfaces (and dust on the surfaces), imperfection of the bulk material, thermal fluctuations in the space charge field [44,45] and thermal fluctuations in the dielectric permittivity associated with the optical Kerr effect [46]. The power of the photon shot noise and noises due to thermal fluctuations can be estimated theoretically [44-46], but the noise intensity due to imperfection of the material is a purely empirical value. Some experimental data, (for instance, [44]) show that the theoretical limits of the photon shot noise and thermal noises are much lower (3-4 orders of magnitude) compared with the experimental data.

So in estimating the information capacity density of volume holograms we shall rely on the data obtained by

different authors at recording of a large number of holograms in one and the same volume of a material. For instance, it follows from [2] and [4] that the information capacity density for volume holographic memory is of the order of $10^6 \div 10^7$ *bit*/mm$^3$. It is interesting that from some theoretical considerations [47] nearly the same value of the information density follows.

Note that the estimates described above give a much lower density of information capacity than that predicted by theory (of the order of $10^{12}$ *bit*/cm$^3$ [48]). The theory does not take into account the noise of the system and states that the information capacity of volume holograms is proportional to $V/\lambda^3$, where $V$ is the volume of the holographic material.

The noise characteristics of photosensitive materials can be described in terms of the dynamic range. This term is used to describe the ratio $P_s/P_n$, but there is no commonly accepted definition for the dynamic range as applied to the information capacity. However, in any situation the limiting value of dynamic range of a material is the main limiting factor in the information capacity of a volume holographic memory system.

Comparing different techniques of recording, we would like to note the advantages of reflection-type holograms because in this case the scattered light can be much lower than for transmission holograms.

Formula (59) describes the information capacity of one page of information. In the case of recording of many holograms in the same volume of a material the optimal number

of pages can be found depending on the information capacity of one hologram and dynamic range of the material. This problem was analyzed in [49].

Below, when we discuss the 1-Tbyte holographic memory, we take the value of the information capacity density of the order of $10^6$-$10^7$.

An example of a hypothetical 1-Terabyte holographic memory system is shown in Fig.23. It includes a $64 \times 64$ array of photorefractive cells, so the magnitude of spatial multiplexing is $M_s = 4096$. Each cell can be approximately $3 \times 3 \times 5$ $mm^3$ in size. The spacing between adjacent cells is about $1$ mm. So the total size (linear dimensions) of the array is $256 \times 256$ $mm^2$. In each cell 700 holograms are recorded. Each hologram or each page of information contains $1024 \times 1024$ pixels with 8 gray levels (3 *bits*). So the capacity of one hologram (one page of information) is $C_p = 0.375$ *Mbytes*. Note that to record these pages of information, liquid crystal spatial light modulators (SLM) can be used. The dynamic range of 3 *bits* is typical of many liquid-crystal SLMs, whereas the number of pixels $1024 \times 1024$ is much higher than the typical magnitude $320 \times 320$ for commercially available inexpensive SLMs. The proposed value of $1024 \times 1024$ is quite realistic from the technical point of view, and it is mostly the problem of price. The magnitude $C_p = 0.375$ *Mbytes* is quite compatible with spectral and electric field multiplexing because the cross-talk between holograms is nearly independent of $C_p$ for these multiplexing techniques. As shown above, when the angular multiplexing technique is used, the cross talk between nearest pages strongly reduces the signal-to-noise ratio. If 700 holograms are recorded in each cell, the amount of information contained in each cell is

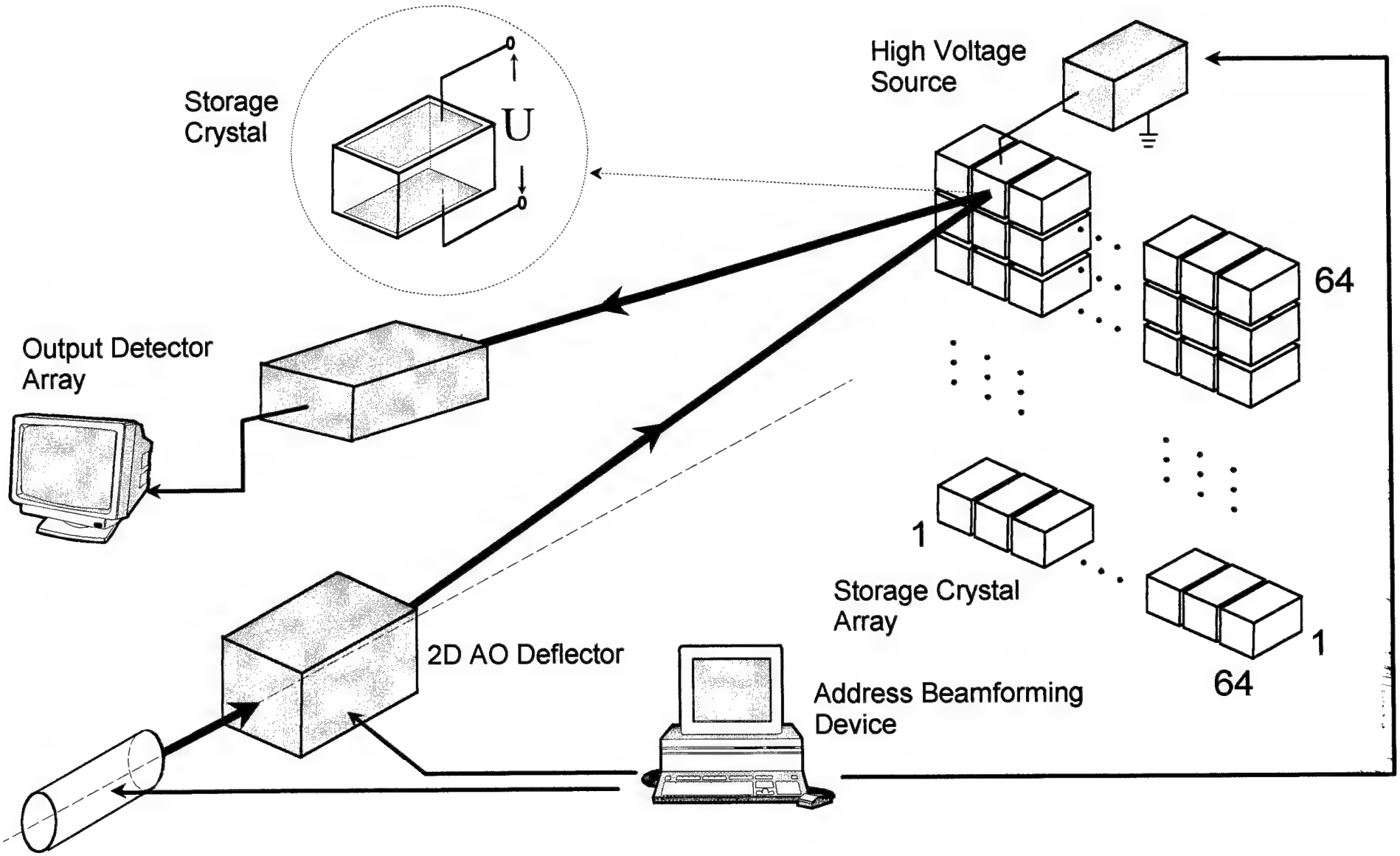


Fig.23 Simplified wavelength, spatial and electric-field multiplexing volume holographic storage system.

about 262.5 *Mbytes*, and the total capacity of the system is 1.025 *Terabyte*. It is assumed that the spectral and electric field multiplexing is used. The reasonable proportion between $M_w$ and $M_{ef}$ is 70/10.

Among other elements, the holographic memory system includes a tunable laser, a two-coordinate acousto-optical deflector, and a source of an external electric field.

The procedure of information retrieval is as follows. A tunable laser is tuned to a proper wavelength and a laser beam is pointed to a definite photorefractive cell by the two-coordinate acousto-optical deflector. Simultaneously, the required external electric field is applied to the photorefractive cell. The reflection hologram geometry is used. The reconstructed image is projected on the detector array (for instance, a CCD camera). In this setup the random access to any hologram in an arbitrary sequence can be provided. It can be quickly accomplished using an AO deflector and by switching the magnitude of the external electric field, but serious problems arise with tunable lasers. The problem of fast random tuning still remains unresolved, but the progress in the area of OPO and semiconductor lasers gives hope that this problem will be solved soon. The required parameters of a tunable laser can be estimated as follows: the minimum distance between two adjacent wavelengths ($\Delta\lambda_0$) is determined by the selectivity of the hologram. For a 5-mm thick hologram and wavelength $\lambda_{r0} = 500$ nm, $\Delta\lambda_0 = 10^{-2}$ nm for $LiNbO_3$. This means

that the laser irradiation bandwidth must be less than $3 \cdot 10^{-3}$ nm, or the coherence length of the laser must be more than 3 cm. However, it is desirable that the interval between two nearest spectral positions (switching step) be more than $\Delta\lambda_0$. Let us select the criterion for the switching step to be equal to $3\Delta\lambda_0$. This is rather an arbitrary criterion, but it provides the necessary low level of overlap between adjacent wavelength positions. Then the total value of the laser tuning range is approximately 20 nm.

This is quite a reasonable value because it constitutes only 4-5% of the average wavelength of irradiation in the visible.

In the case when the laser with the characteristics mentioned above and with a high switching speed is available, there is no necessity to use electric field multiplexing, but in other cases the electric field multiplexing can facilitate reaching the necessary total multiplexing which is admitted to be a few hundreds. It is necessary to note that the electric field and spectral multiplexing are not quite independent in the sense that the shift of the refractive index by the external electric field can be compensated for by a proper change in the wavelength to satisfy the Bragg condition. This means, in particular, that if we use the electric field multiplexing with $M_{ef}$, the wavelength shift between the adjacent wavelength positions must be $30\Delta\lambda_0$ to escape compensation between the change in the electric field and spectral tuning. However, the accuracy of the

spectral positioning and bandwidth of the laser radiation which is less than $\Delta\lambda_0$ must remain the same.

Concerning a real holographic memory system, we should like to mention two more problems. They are the throughput of the system and optical elements. The throughput of the system ($H$) at the information readout can be estimated as

$$H = \frac{C_p}{\tau_p} \tag{60}$$

where $\tau_p$ is the random access time. Then for the capacity of the order of $C_p = 0.4\,Mbyte$ and $\tau_p = 1$ ms, $H$ is of the order of 3 *Gbit*/s. The sophisticated equipment is required to convert the optical data into electronic signals and transmit the data. The compromise can be reached at the cost of longer access time.

The other serious problem is the optical elements of the system. A large size of the array of photorefractive cells and a small size of 1 pixel (less than 30 μm) require very precise and distortion-free optical elements, and objectives, in particular. However, it is possible to find more optimal configurations with a smaller size of the array of photorefractive cells. The radical improvement can be reached by increasing the dynamic range of the photosensitive holographic material. The materials with higher characteristics than $LiNbO_3$ is the key problem for this technique.

## *Conclusions*

In the final report the results of investigation in accordance with the requirements of the contract are presented. All the necessary subjects have been investigated. The main results are as follows:

1) The spectral selectivity of the reflection hologram has been analyzed theoretically and checked experimentally. The obtained experimental results for $LiNbO_3$ have shown that the selectivity better than $1 \div 1.5$ **A** can be easily reached.

2) Two sources of cross-talk at spectral multiplexing have been analyzed. They are the cross-talk due to the complicated structure of the recorded image and the cross-talk due to the limited coherence of the readout light.

3) The comprehensive mathematical analysis of the cross-talk due to the limited coherence of the readout light has been carried out and it has been shown that this factor can play a crucial role in the wavelength multiplexing.

4) The numerical calculations of the dependences of cross-talk on the width of the readout light spectrum and on the quantity of recorded holograms have been performed. These data allow one to draw recommendations concerning the optimization of the hologram recording conditions for each particulat case. In the simplest situation, it is necessary to satisfy the following requirements:

a) $\delta\lambda/\Delta\lambda_0 < 1/3$; and

b) the accuracy of the wavelength positioning should be better than $\Delta\lambda_0$.

5) A required setup for the experimental investigations of the electric field multiplexing has been built and properly cut, oriented, and polished single crystals of $LiNbO_3$ have been prepared.

6) An efficient configuration for recording reflection holograms which provides a high diffraction efficiency and efficient electric control has been found for $LiNbO_3$. The required theoretical calculations and experiments have been performed.

7) A theory for the electric field selectivity in photorefractive materials has been developed. The comparsion of theoretical calculations with the experimental data exibits an excellent agreement at the certain conditions.

8) The experiments have shown that the electric field inhomogeneity plays an important role in reduction of the electric field selectivity.

9) The investigations have shown that the electric field multiplexing of the order of 20 is realistic.

10) The analysis of the role of scattered light in the dynamic range of photorefractive materials has shown that the limited dynamic range of the material is one of the main problems to be solved for manufacturing high-capacity holographic memories.

11) A simplified version of the 1-*Tbyte* holographic memory system has been presented.

Finally, the general recommendations can be formulated.

The Terabyte holographic memory can be built, but two major problems have to be solved. The first one is developing the holographic materials with better dynamic range to have the information capacity density of the order of $10^7$-$10^8$ *bit*/mm$^3$. Otherwise, a too high bit-error rate of the system will result, or the system size will be beyond the reasonable scale.

The second important problem is a tunable laser. Quite a moderate coherence (the bandwidth of the laser radiation of the order of $3 \cdot 10^{-3}$ nm) is required. However, fast (of the order $10^{-3}$ s) switching of the generated wavelength is desirable in a random sequence, with the accuracy of the wavelength positioning better than $10^{-2}$ nm. The total number of fixed wavelength positions must be of the order of $10^3$ and the interval between the nearest spectral positions must be $0.3 \div 1 \cdot 10^{-1}$ nm.

## *References*


1. Terabyte Holographic Memory, Interim Report, Contract F61708-96-W0308 (1997).

2. J.H.Hong, I.McMichael, T.Y.Chang, W.Christian, E.Gi Paek, Optical Eng., 34, No.8 (1995), 2193-2203.

3. W.J.Burke and P.Seng, J.Appl.Phys., 48 (1977) 481.

4. L. Hesselink, M.C. Bashaw, Opt. and Quant. Electr., 25 (1993) S611.

5. M.C.Bashaw, J.F. Heanue, A.Aharani, J.F.Walkup, L.Hesselink, J. Opt.Soc.Am. B 11 (1994) 1820-1836.

6. R.J.Collier, B.Burckhardt, and L.H.Lin, Optical Holography, Academic Press, 1971.

7. G.Gu.Hong, I.McMichael, R.Saxena, and F.H.Mok, J.Opt.Soc.Am. A 9 (1992) 1973.

8. S.Wu and Q.Song, Appl.Opt., 29 (1990) 1113.

9. J.M.Heaton, P.A.Mills, E.G.S.Paige, L.Solymar, T.Wilson, Opt. Acta, 31 (1984) 885.

10. H.Mok, M.C.Tackitt, and H.M.Stoll, Opt.Lett., 16 (1992), 605.

11. F.H.Mok, Opt.Lett., 18 (1993), 915-917.

12. F.H.Mok, D.Psaltis, and G.Burr, Proc.Soc.Photo-Opt. Instrum. Eng., 1773 (1992) 334.

13. D.Psaltis, C.Gu, and D.Brady, Proc.Soc.Photo-Opt.Instrum.Eng., 963 (1988) 70.

14. S.Tao, D.R.Selviah, and J.E.Midwinter, Opt.Lett., 18 (1993) 912.

15. J.V.Alvarez-Bravo, N.Bolognini, and L.Arizmendi, Appl.Phys. B 62 (1996) 159.

16. C.Denz, G.Pauliat, G.Roosen, T.Tschudi, Opt.Commun., 85 (1991), 171-176.

17. K.Curtis, D.Psaltis, JOSA A, 10 (1993), 25-47.

18. H.Sasaki, J.Ma, Y.Fainman, S.H.Lee, Y.Taketomi, Opt.Lett., 17 (1992), 1468-1470.

19. I.Lorgege, F.Grelet, M.Ratsep, M.Tian, J.L.LeGouet, C.Sigel, M.L.Roblin, JOSA,B, 13 (1996), 2229-2234.

20. M.C.Bashaw, R.C.Singer, J.F.Heanue, L.Hesselink, Opt.Lett., 20 (1995), 1916-1918.

21. C.A.Rakuljic, V.Leyva, A.Yariv, Opt.Lett., 17 (1992), 1471-1474.

22. A.Yariv, Opt.Lett., 18 (1993), 652-654.

23. S.Yin, H.Zhou, F. Zhao, M.Wen, Z.Yang, and F.T.S.Yu, Opt. Commun., 101 (1993) 317.

24. J.H.Jang, Y.H.Kang, H.Lee, Opt.Lett., 20 (1995), 2426-2428.

25. T.Kume, K.Nonaka, M.Yamamoto, CLEO'96, Proceedings, CTuM5.

26. A.J.Herderson, M.J.Padgett, F.G.Colwille, J.Zhang, M.H.Dunn, Opt.Commun., 119 (1995), 256-264.

27. F.Huisken, M.Kaloudis, J.Marquez, Yu.L.Chuzavkov, S.N.Orlov, Yu.N.Polivanov, V.V.Smirnov, Opt.Lett., 20 (1995), 2306-2308.

28. I.Zawischa, A.I.Ferguson, Opt.Lett., 21 (1996), 45-47.

29. K.Curtis, C.Gu, D.Psaltis, Opt.Lett., 18 (1993), 1001-1003.

30. H.W.Kogelnik, Bell Syst. Tech. J., 48 (1969), 2909.

31. J.F.Heanue, M.C.Bashaw, L.Hesselink, J. Opt. Soc. Am. A, 12 (1995), 1671

32. Yu.L.Korzinin, V.I.SuKhanov Opt. Spectrosc. (in Russian), 56 (1984) 763.

33. A.Kewitsch, M.Segev, A.Yariv, R.R.Neurgaonkar, Opt.Lett., 18 (1993) 534.

34. R.De Vre, M.Jeganathan, J.P.Wilde and L.Hesselink, J.Opt.Soc.Am. B, 12(1995) 600.

35. J.V.Alvarez-Bravo, R.Muller and L.Arizmendi, Europhys. Lett., 31 (1995), 443.

36. K.Sayano, F.Zhao, S.T.Hendow and N.V.Kukhtarev, Post-deadline paper at CLEO'96, June 2-7, 1996, Anaheim, CA.

37. A.A.Kamshilin, M.P.Petrov, S.I.Stepanov, A.V.Khomenko, Avtometriya (in Russian) 1(1978), 16.

38. M.P.Petrov, S.I.Stepanov, A.A.Kamshilin, Ferroelectrics 21, (1978), 631.

39. M.P.Petrov, S.I.Stepanov, A.A.Kamshilin, Opt.Commun. 29 (1979), 44.

40. M.Born, E.Wolf, Principles of Optics, Pergamon Press, 1968, 719 pp.

41. P.B.Fellgett, E.H.Linfoot, Phil.Trans.Roy.Soc., A247 (1955), 369.

42. M.P.Petrov, S.I.Stepanov, A.V.Khomenko, Photorefractrive Crystals in Coherent Optical Systems, Springer Verlag, 1991.

43. S.V.Miridonov, A.V.Khomenko, D.Tentori, A.A.Kamshilin, Opt.Lett., 19 (1994), 502.

44. T.Y.Chang, J.H.Hong, F.Vachss, R.McGraw, JOSA, B, 9 (1991), 1744.

45. C.Gu, P.Yeh, Opt.Lett., 16 (1991), 1572.

46. R.McGraw, Phys.Rev., A42 (1990), 2235.

47. R.G.Zech, Opt.Photon.News, 3 (1993), 16.

48. P.J.Van Heerden, Appl.Opt., 2 (1963), 393.

49. Yu.I.Kuz'min, Pis'ma v Zh.Tekh.Fiz. (in Russian), 23 (1997), 18.